Quantum-chaotic scattering effects in semiconductor microstructures

Harold U. Baranger, Rodolfo A. Jalabert, and A. Douglas Stone

Citation: Chaos: An Interdisciplinary Journal of Nonlinear Science **3**, 665 (1993); doi: 10.1063/1.165928
View online: http://dx.doi.org/10.1063/1.165928
View Table of Contents: http://scitation.aip.org/content/aip/journal/chaos/3/4?ver=pdfcov
Published by the AIP Publishing

Quantum-chaotic scattering effects in semiconductor microstructures

Harold U. Baranger
AT&T Bell Laboratories 1D-230, 600 Mountain Avenue, Murray Hill, New Jersey 07974-0636

Rodolfo A. Jalabert
Division de Physique Théorique,[a] Institut de Physique Nucléaire, F-91406 Orsay Cedex, France

A. Douglas Stone
Applied Physics, Yale University, P.O. Box 208284, New Haven, Connecticut 06520-8284

(Received 30 July 1993; accepted for publication 13 October 1993)

We show that classical chaotic scattering has experimentally measurable consequences for the quantum conductance of semiconductor microstructures. These include the existence of conductance fluctuations—a sensitivity of the conductance to either Fermi energy or magnetic field—and weak-localization—a change in the average conductance upon applying a magnetic field. We develop a semiclassical theory and present numerical results for these two effects in which we model the microstructures by billiards attached to leads. We find that the difference between chaotic and regular classical scattering produces a qualitative difference in the fluctuation spectrum and weak-localization lineshape of chaotic and nonchaotic structures. While the semiclassical theory within the diagonal approximation accounts well for the weak-localization lineshape and for the spectrum of the fluctuations, we uncover a surprising failure of the semiclassical diagonal-approximation theory in describing the magnitude of these quantum transport effects.

I. INTRODUCTION

During the past decade significant progress has been made in the study of quantum systems whose classical analogs exhibit chaotic dynamics.[1] However most of the progress in this emerging subject of "quantum chaos" has consisted in the development of theoretical concepts; there are currently very few experimental measurements which test these new ideas. Some time ago we suggested that low-temperature transport measurements in microstructures could provide a new and controllable system for the comparison of theory and experiment in the area of quantum-chaotic scattering.[2] Of particular interest were measurements of novel high-mobility semiconductor (GaAs/AlGaAs) heterostructures, for which disorder-scattering may be neglected in comparison to the scattering from geometric features along the conducting path.

Within condensed matter physics interest in the physics of "mesoscopic" conductors (i.e. conductors small enough to be treated as a single phase-coherent unit) has been strong for some time.[3] Typically such conductors will have static defects which generate bulk disorder scattering and an *elastic* mean free path much less than the device dimensions; however, this is not the case for the high-mobility structures just mentioned, in which both the elastic and inelastic mean free paths exceed relevant device dimensions at low temperatures. Nonetheless, the extensive previous study of disordered microstructures and of quantum transport phenomena in macroscopic solids suggested that effects related to interference of multiply reflected electron waves would be important. In disordered phase-coherent conductors two such phenomena were already well-known: (1) *Weak-Localization*, a decrease in the average conductance due to constructive interference of time-reversed backscattering trajectories.[4] (2) *Universal Conductance Fluctuations*, reproducible fluctuations in the conductance versus magnetic field or Fermi energy with rms size of order e^2/h, independent of the average conductance.[5,6] Because "disordered" potentials may be regarded as generating chaotic dynamical systems specified by a large number of parameters (e.g. impurity locations and scattering strengths), it is natural to look for analogs of these effects in the simpler chaotic potentials realizable in ballistic microstructures. Several interesting questions could be addressed in such systems. (1) How similar are the statistical properties of the conductance of ballistic and disordered microstructures? (2) In ballistic microstructures can the quantum interference effects be related to properties of the relevant classical phase space? (3) How do the statistical properties of the conductance in microstructures with integrable or nearly integrable potentials differ from those with chaotic potentials? We present theoretical results relating to these questions below.

In the case of disordered conductors there is already a wealth of experimental data relating to the weak-localization and universal conductance fluctuation effects; however, these are not very relevant to the three questions just stated. The application of semiclassical methods to quantum problems is interesting primarily as a means of connecting quantum properties to specific features of the classical dynamics of a system. Obviously, in disordered conductors the potential generating chaotic motion is not known in any detail and comparisons of this type are not possible. Moreover, whereas in simple chaotic systems the only length scale is the system size L, in disordered conductors there is an additional length scale, l, the elastic

[a]Unité de Recherche des Universités Paris XI et Paris VI associée au CNRS.

 1054-1500/93/3(4)/665/18/$6.00

scattering length. It is now known that the existence of this second scale causes deviations from the universal behavior typical of quantum-chaotic systems and describable by random-matrix theory.[7,8] Hence meaningful experimental tests of the semiclassical theory of chaotic (or nearly integrable) quantum systems require high-mobility nanostructures patterned with enough control of the sample geometry to make such comparisons reasonable. Since the publication of our initial results, several groups have accepted the challenge of such a difficult experimental program[9–14] and some of their results are reviewed elsewhere in this issue.[15] Although these results have several encouraging features, it is clear that there is much of value to be gained by further and more refined experiments.

The physical property of these nanostructures which is most easily measured experimentally is their electrical resistance. Because this resistance does not arise from phonon or impurity scattering it is *not* related to an intensive resistivity of the type defined in standard text books on solid-state physics.[16] Instead one must treat the entire conductor as a phase-coherent unit which generates quantum scattering of an incident current. This point of view, which was developed in the work of Landauer and Büttiker,[17,18] leads to the conclusion that resistance measurements on microstructures on a length scale shorter than the *inelastic* mean free path can be related to simple quantum scattering problems. We review these arguments briefly below.

First we recall the justification for neglecting the strong interactions between the conduction electrons. As argued originally by Landau, although the conduction electrons in a typical solid interact strongly through their Coulomb repulsion, as long as the system retains a discontinuity in the equilibrium occupation numbers at a certain energy E_F (i.e. has a Fermi surface) there exist particle-hole excitations whose lifetime goes to infinity as $T\to 0$ and $E\to E_F$.[16] This is the essential idea of Fermi liquid theory, and it means that the properties of normal metals at or below room temperature are qualitatively similar to those of a noninteracting Fermi gas coupled to lattice vibrations (phonons). At temperatures of order one Kelvin the inelastic mean free path for phonon-scattering (or residual electron–electron scattering) becomes very long compared to the elastic mean free path and metals in the normal state are well-described by models of noninteracting fermions moving in a *static* potential. Usually this potential is determined primarily by impurities, but in ballistic microstructures it will be determined by the boundaries of the conducting regions. If one measures the conductance of a microstructure for which the electron transit time is short compared to the inelastic scattering time then the conduction process can be viewed as the coherent quantum-mechanical transmission of independent particles. The conductance associated with this transmission process can be evaluated by a counting argument;[17,18] the same result can be obtained from linear response theory.[19–21]

The basic physical idea of this approach is to consider the microstructure in this regime as a single phase-coherent unit attached to ideal electron reservoirs which represent the much larger electrical contacts whose resistance is negligible compared to that of the sample. In an ideal *two-probe measurement* the sample is attached between two perfect reservoirs with electrochemical potentials μ_1 and $\mu_2=\mu_1-eV$, respectively (where V is the applied voltage), and these reservoirs serve both as current source and sink *and* as voltage terminals. In the energy interval eV between μ_2 and μ_1 electrons are injected into right-going states emerging from reservoir 1, but none are injected into left-going states emerging from reservoir 2. Thus there is a net right-going current proportional to the number of states in the interval $\mu_1-\mu_2$, given by

$$I=e\sum_{m=1}^{N_M} v_m \frac{dn_m}{d\varepsilon} eV \sum_{n=1}^{N_M} T_{nm}=\left(\frac{e^2}{h}\right)\sum_{n,m=1}^{N_M} T_{nm}V, \tag{1}$$

where N_M is the number of propagating channels including spin *in the sample*, v_m is the longitudinal velocity for the mth momentum channel at the Fermi surface, T_{nm} is the transmission probability from m to n, and we have used the fact that for noninteracting particles the quasi-one-dimensional density of states satisfies $dn_m/d\varepsilon=1/hv_m$. Equation (1) shows that the two-probe conductance is just proportional to the total transmission coefficient of the microstructure,

$$G=\frac{e^2}{h}\sum_{n,m=1}^{N_M} T_{nm}\equiv\frac{e^2}{h}T. \tag{2}$$

It is often convenient to use reflection coefficients, defined analogous to the transmission coefficients. Note that the normalization condition on these transmission and reflection coefficients is $T+R=N_M$ (this follows from the unitarity of the S-matrix).

Hence two-probe conductance measurements directly probe the quantum S-matrix describing the multiple-scattering from the entire sample treated as a single composite scatterer. This is also true for four-probe transport measurements such as Hall resistance; however, the theoretical description is somewhat more complicated since then a matrix of conductance coefficients must be introduced.[18,20,21] The experiments on quantum chaos in microstructures undertaken to date have been essentially two-probe measurements[9–12] and the simple description of Eq. (2) is the relevant one.

From the point of view of the general theory of quantum chaos, the treatment of quantum-chaotic scattering requires some novel analysis. Most of the effort in quantum chaos during the past decade has focused on semiclassical derivations of quantum spectral properties, using the Gutzwiller trace formula[1] or its more recent refinements.[22] For example, it has been shown[23] that the two-point spectral correlations of chaotic systems are well-described by Wigner–Dyson random matrix theory over an energy interval E such that $\Delta\ll E\ll\hbar/T_0$ where Δ is the level spacing and T_0 is the period of the shortest periodic classical orbit. Moreover, extensive numerical investigations show that many other spectral statistics of chaotic systems (such as the nearest neighbor spacing distribution) are well-described by random-matrix theory.[24] In addition, spectral correlations on a scale $E\approx\hbar/T_0$ may be obtained from a

semiclassical analysis which only takes into account a few short orbits, and striking successes of this approach have been demonstrated for, e.g., the hydrogen atom in a magnetic field.[25] Much less is known analytically about the *properties of the eigenfunctions* of classically chaotic systems. This makes the study of quantum-chaotic scattering[26] particularly interesting because the quantum S-matrix depends in an essential way on the properties of the wave functions.

In addition, consideration of scattering problems introduces into the theory a new time scale, τ_0, the mean escape time from the scattering region. In quantum scattering problems where the escape occurs via tunneling, τ_0 cannot be derived from straightforward consideration of the classical dynamics (although it can be treated semiclassically by going to imaginary time and inverting the potential). However in problems of the sort we will be considering, in which a particle is injected into a cavity, bounces many times and ultimately escapes, the escape time is a purely classical quantity which we obtain by simulation of the classical equations of motion for a distribution of initial conditions. One may still consider two limits in this case. If the apertures through which particles can escape become very small, $\hbar/\tau_0$ can become less than the level spacing Δ of the closed cavity. In this case one observes strong resonances whose properties may be described by the semiclassical spectral theory. In semiconductor microstructures this regime may be probed in experiments on "quantum dots", nearly isolated islands of electron gas, connected to leads through tunnel barriers or narrow constrictions. The analysis of conductance resonances in this case is complicated by the presence of large Coulomb charging energies for adding an electron to the dot, and by thermal broadening of the resonances. However it has been recently predicted that the distribution of resonance amplitudes should reflect the underlying chaotic nature of the eigenstates,[27,28] and experimental tests of this hypothesis are expected in the near future.

In the current work, however, the case of primary interest is when $\hbar/\tau_0 \gg \Delta$ and weak overlapping "resonances" occur;[26] in this regime one cannot associate peaks in the transmission with individual levels and indeed the whole notion of *the* spectrum of the system becomes ill-defined since there is no natural choice of boundary conditions to impose. This regime has been extensively studied in the nuclear physics literature where it is known as the Ericson fluctuation regime.[24,29] In this case the new energy scale $\hbar/\tau_0$ enters into the semiclassical theory in a fundamental manner,[30] and the semiclassical theory of chaotic spectra is not of obvious relevance. Below we will review and extend our results for the conductance of such ballistic microstructures.[2,31–33] We study the ballistic analogs of weak-localization and universal conductance fluctuations and are able to relate these statistical properties to features of the classical dynamics. This is done by a combination of approximate semiclassical calculations and exact quantum and classical numerical simulations. In particular we are able to show that such measurements can distinguish between chaotic and nearly integrable scattering potentials.

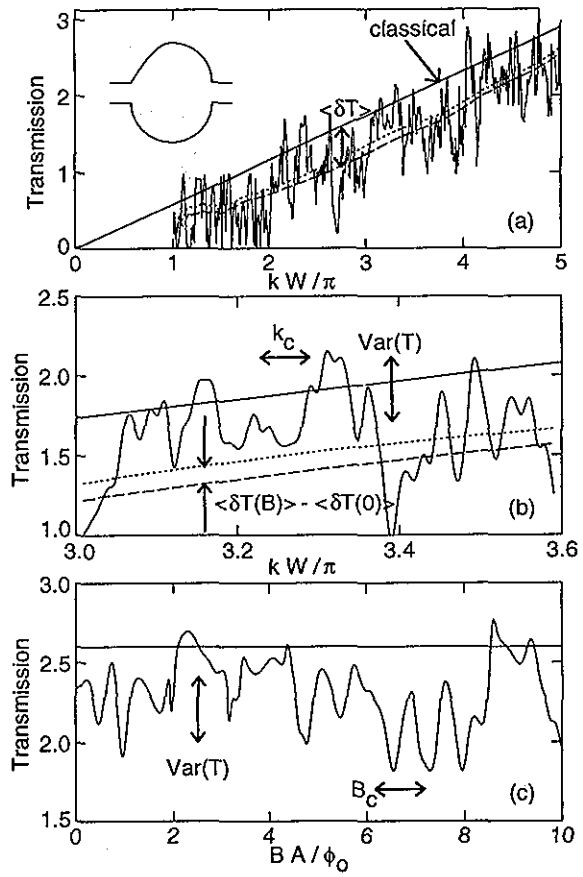

FIG. 1. Transmission coefficient as a function of wave vector [(a) and (b)] or magnetic field [(c)] through the cavity shown in panel (a). In all the panels, the straight solid line is the classical transmission T_{cl}, the fluctuating solid line is the full quantum transmission T_{qm}, and the dashed (dotted) line is the smoothed T_{qm} at $B=0$ ($BA/\phi_0=0.25$). Note the following four main effects. (1) The smoothed T_{qm} increases with the same slope as T_{cl} [(a)]. (2) The smoothed T_{qm} is smaller than T_{cl} by a substantial amount, $\langle \delta T \rangle$[(a)], which is sensitive to B [(b)] and therefore constitutes an average magnetoconductance. (3) T_{qm} fluctuates by an amount of order unity as a function of both k and B: $var(T) \sim 1$ [panels (a)–(c)]. (4) The spectrum of T_{qm} has a characteristic scale, k_c or B_c, which can be related to classical quantities. (W is the width of the leads, and A is the area of the cavity.)

However our semiclassical analysis, which is based on approximations very similar to those used in the theory of chaotic spectra, only gives qualitative agreement for the magnitude of the weak-localization and universal conductance fluctuations. This suggests that the theory of quantum-chaotic S-matrices will require a significant extension of semiclassical theory.

Before we present the semiclassical theory, we illustrate in Fig. 1 the main effects that we will be discussing: numerically computed $T(k)$ and $T(B)$ curves are shown for an asymmetrized stadium in both the classical and quantum limits. The transmitted flux increases linearly as a function of k as the incident flux ($\propto kW/\pi$) increases [panel (a)]. The average quantum result lies below the classical curve, largely because of mode effects from confinement in the leads. However, part of this offset is sensitive to a weak magnetic field; this is the weak-localization

effect [panel (b)]. Perhaps the most striking feature of Fig. 1 is the fine structure in the quantum curve. These are the conductance fluctuations which we will characterize in terms of both their magnitude, $var(T)$, and their correlation scales k_c for $T(k)$ and B_c for $T(B)$.

II. SEMICLASSICAL TRANSMISSION COEFFICIENTS

As noted above, ballistic microstructures represent a condensed matter system where one may hope to apply detailed semiclassical analysis to describe quantum properties in terms of properties of the classical phase space. The semiclassical Green functions are the natural link between quantum and classical physics (particularly in the chaotic regime where the phase-space has no invariant tori and Bohr–Sommerfeld quantization cannot be employed). These Green functions are expressed as sums over classical trajectories whose actions and stabilities determine the associated phases and weights. The Green function in which we are interested is that related to the transmission (and reflection) amplitudes between any two modes m to n and is therefore related to the transmission probabilities T_{nm} appearing in Eq. (2).

The transmission (reflection) amplitude from a mode m on the left to a mode n on the right (left) for electrons at the Fermi energy E is given by the projection of the retarded Green function (evaluated at the Fermi energy) over the transverse wave functions ϕ_m and ϕ_n of the incoming and outgoing modes.[19]

$$t_{nm}=-i\hbar(v_n v_m)^{1/2}\int dy'\int dy\,\phi_n^*(y')\phi_m(y) \times G(L,y';0,y;E), \tag{3a}$$

$$r_{nm}=\delta_{nm}-i\hbar(v_n v_m)^{1/2}\int dy'\int dy\,\phi_n^*(y')\phi_m(y) \times G(0,y';0,y;E). \tag{3b}$$

The intuitive interpretation of the above equations as arriving at the cavity in mode m, propagating inside the cavity (through the Green function), and exiting in mode n is quite straightforward.

These equations constitute an exact starting point which is also the basis of our numerical calculations. As described in detail in Ref. 31, we obtain the Green function of a tight-binding Hamiltonian (equivalent to a real-space discretization of the Schrödinger equation) by a recursive algorithm and then do a (discrete) projection onto the transverse wave functions in the leads. This yields, then, the exact transmission amplitude of the discretized problem and the conductance follows from Eq. (2).

The semiclassical approximation to the transmission and reflection amplitudes proceeds by replacing the Green function G by its semiclassical path-integral expression[1]

$$G^{\rm scl}(y';y;E)=\frac{2\pi}{(2\pi i\hbar)^{(3/2)}}\sum_{s(y,y')}\sqrt{D_s} \times\exp\left(\frac{i}{\hbar}S_s(y',y,E_F)-i\frac{\pi}{2}\mu_s\right), \tag{4}$$

given as a sum over classical trajectories s between points y and y' of the entrance and exit cross sections (hereafter we will not write any x dependence). S_s is the action integral along the path, $D_s=(v|\cos\theta'|/m)^{-1}|(\partial\theta/\partial y')_y|$, θ and θ' are the incoming and outgoing angles, and μ is the Maslov[1] index given by the number of constant-energy conjugate points.

In the case of hard-wall leads, the transverse wave functions have a sinusoidal form: $\phi_m(y)=\sqrt{2/W}\sin(m\pi y/W)$. For large m the integral over y will be dominated by the stationary-phase contribution occurring for trajectories starting at points y_0 defined by

$$\left(\frac{\partial S}{\partial y}\right)_{y'}=-p_y=-\frac{\bar{m}\hbar\pi}{W},\quad \bar{m}=\pm m, \tag{5}$$

that is, the dominant trajectories are those for which the initial transverse momentum equals the momentum of the transverse wave function. Performing also the y' integral by stationary-phase, we obtain

$$t_{nm}=-\frac{\sqrt{2\pi i\hbar}}{2W}\sum_{s(\bar{n},\bar{m})}\mathrm{sgn}(\bar{n})\mathrm{sgn}(\bar{m})\sqrt{D_s} \times\exp\left(\frac{i}{\hbar}\tilde{S}_s(\bar{n},\bar{m},E)-i\frac{\pi}{2}\tilde{\mu}_s\right) \tag{6}$$

where the sum is now taken over trajectories s between the entrance and exit cross sections with incoming and outgoing angles θ and θ' such that $\sin\theta=\bar{m}\pi/kW$ and $\sin\theta'=\bar{n}\pi/kW$. The reduced action is

$$\tilde{S}(\bar{n},\bar{m},E)=S(y_0',y_0,E_F)+\hbar\pi\bar{m}y_0/W-\hbar\pi\bar{n}y_0'/W, \tag{7}$$

the new pre-exponential factor is

$$\tilde{D}_s=\frac{1}{mv|\cos\theta'|}\left|\left(\frac{\partial y}{\partial\theta'}\right)_\theta\right|, \tag{8}$$

and the new Maslov index is

$$\tilde{\mu}=\mu+H\left(-\left(\frac{\partial\theta}{\partial y}\right)_{y'}\right)+H\left(-\left(\frac{\partial\theta'}{\partial y'}\right)_\theta\right), \tag{9}$$

where H is the Heaviside step function.

When taking the semiclassical limit by increasing the Fermi energy the trajectories contributing to t_{nm} will change as larger Fermi wave vectors give smaller injection angles for a given mode number m. On the contrary, if we look at Eq. (6) as the transmission amplitude between the directions of θ and θ', the trajectories contributing will remain unchanged in billiard-like structures as we move into the semiclassical limit (apart from a trivial energy scale factor).

Similar arguments can be used to write the semiclassical reflection amplitude in terms of trajectories leaving and returning to the cross section at $x=0$ with appropriate quantized angles. Note that there are two kinds of trajectories contributing to $G^{\rm scl}(y';y;E)$ in the case of reflected paths: those which penetrate into the cavity and those which go directly from y to y' staying on the cross section of the lead. Clearly it is only trajectories of the first kind

which contribute to the semiclassical reflection amplitude as trajectories of the second kind merely cancel the δ_{nm} of Eq. (3b).

Some special care must be taken for structures in which there are direct trajectories between the incoming and outgoing leads. The semiclassical transmission amplitude of Eq. (6) assumes that the contributing trajectories are all isolated, and some modification is needed to include the effect of the family of direct trajectories. For the diagonal contribution t^{d}_{mm} of the direct trajectories we can follow the same procedure as before and perform the integral over y by stationary-phase approximation, yielding

$$t^{\mathrm{d}}_{mm}=\frac{i}{W}\left\{\int_{L\tan\theta}^{W} dy'\phi_m(y')\exp\left(i\left(\frac{kL}{\cos\theta}+\frac{\pi m y_0}{W}\right)\right)\right.$$
$$\left.-\int_{0}^{W-L\tan\theta} dy'\phi_j(y')\exp\left(i\left(\frac{kL}{\cos\theta}-\frac{\pi m y_0}{W}\right)\right)\right\}, \tag{10}$$

where $L/\cos\theta$ is the length of all the trajectories, $y_0=y'-L\tan\theta$ is the intial point of the trajectory reaching the exiting cross section at y', $\sin\theta=\bar{m}\pi/kW$ and the Maslov index is zero. Of course, we cannot perform as before the integral over y' by stationary-phase as there is no quadratic term in the action. However we can calculate the integral in closed form obtaining

$$t^{\mathrm{d}}_{mm}=-\exp\left(\frac{ikL}{\cos\theta}\right)\left\{\left(1-\frac{L}{W}\tan\theta\right)\exp\left(-i\pi m\frac{L}{W}\tan\theta\right)\right.$$
$$\left.+\frac{1}{\pi m}\sin\left(\pi m\frac{L}{W}\tan\theta\right)\right\}. \tag{11}$$

For large quantum numbers m we can neglect the last (small and rapidly oscillating) term.

In an analogous way we can compute the off-diagonal contribution t^{d}_{nm} of the direct trajectories, given in the large n and m limit by

$$t^{\mathrm{d}}_{nm}=-\frac{1}{2\pi}\left|\frac{\cos\theta_n}{\cos\theta}\right|^{1/2}\cdot\exp\left(i\left(\frac{kL}{\cos\theta}-\pi\frac{(n+m)}{2}\frac{L}{W}\tan\theta\right)\right)$$
$$\times\sin\frac{\{\pi[(n-m)/2](L/W)\tan\theta\}}{(n-m)}. \tag{12}$$

As expected the result is strongly peaked for $n=m$ [where Eq. (11) should be used], but shows nevertheless an important off-diagonal contribution for close quantum numbers n and m.

It is important to notice the different dependence on $\hbar$ (or k) for the contribution from the family of direct trajectories and the isolated trajectories; the former dominating in the limit $k\to\infty$. The existence of direct trajectories thus complicates the comparison between experiment (both numerical and laboratory) and the semiclassical theory. Thus in many of our numerical simulations we have introduced "stoppers" in the billiards which eliminate this effect; the experimentalists have also tried to avoid this problem by displacing the leads[10] or having an angle smaller than π between them.[9] Even if we can circumvent the problem of the direct trajectories by going to more complicated structures the special character of the semiclassical contribution of a family of trajectories will remain for integrable structures like rectangles. The contribution of families of trajectories in cavities with straight sides is more complicated to evaluate than for direct trajectories, but nevertheless we can anticipate that they will have the same dependence on $\hbar$ and cause integrable scattering systems to approach the classical limit differently from chaotic scattering systems.

For the scattering problem the semiclassical contributions in the chaotic [Eq. (6)] and direct trajectory [Eq. (11)] cases are the analog, respectively, of the contributions of isolated periodic orbits and a family of periodic orbits to the density of states.[1] The main difference between the scattering and energy-level problems at the semiclassical level is that the trace formula for the density of states involves the sum over periodic orbits while the transmission amplitude is given by open trajectories that traverse the scattering region. The fact that the open trajectories escape from the scattering region implies that the semiclassical transmission sum will not be complicated by the convergence problems[1,22] of the trace formula. From the quantum point of view, because the Gutzwiller trace formula must reproduce a delta-function spectrum, it can be at most conditionally convergent, while the quantum transmission amplitude is a smooth function of the Fermi energy (away from thresholds for modes in the leads[34]) and so the semiclassical sum can be absolutely convergent. Convergence of semiclassical propagators in chaotic scattering problems has recently been addressed by Jensen.[35]

Chaotic scattering problems for potentials which asymptotically go to zero have often been studied in terms of the semiclassical propagator in the momentum representation, first discussed by Miller[36] starting from canonical transformations. The relevant sum in this case is over classical trajectories with fixed incident and outgoing momenta, similar but not identical to what we find for the transmission amplitude in our "waveguide" geometry. Our procedure gives a more explicit semiclassical formula for use in the Landauer–Büttiker conductance formulas and allows one to handle more complicated situations like families of trajectories, soft walls in the leads[31] and magnetic field.[33] In particular we obtain a prescription for evaluating the Maslov indices, making possible numerical evaluation of the semiclassical transmission amplitude by direct summation in cases of interest.[33] While we do not pursue direct summation of semiclassical expressions here, we note that it has proved valuable in the context of closed billiards[37] and could be used to clarify some of the issues discussed below.

Transmission coefficients (or probabilities) between modes are obtained by taking the magnitude squared of the transmission amplitudes, $T_{nm}=|t_{nm}|^2$. They will therefore be given as sums over *pairs* of trajectories. Since we will be focusing on billiards it is convenient to scale out the energy (or momentum) dependence and use the notation

$$T(k)=\sum_{n=1}^{N_M}\sum_{m=1}^{N_M}T_{nm}=\frac{1}{2}\frac{\pi}{kW}\sum_{n,m}\sum_{s}\sum_{u}F^{s,u}_{n,m}(k), \tag{13}$$

$$F^{s,u}_{n,m}(k)=\sqrt{\widetilde{A}_s\widetilde{A}_u}\exp[ik(\widetilde{L}_s-\widetilde{L}_u)+i\pi\phi_{s,u}], \qquad (14)$$

where s and u label the paths with extreme angles θ and θ', the effective length is $\widetilde{L}_s=\widetilde{S}_s/k\hbar=S_s/k\hbar+y\sin\theta-y'\sin\theta'$, the Maslov indices are included in the phase-factor $\phi_{s,u}=(\widetilde{\mu}_u-\widetilde{\mu}_s)/2$, and $\widetilde{A}_s=(\hbar k/W)\widetilde{D}_s$. In writing Eq. (13) and Eq. (14) we assume the transmission amplitudes are given by Eq. (6), that is to say, we are not considering the contribution of direct trajectories [Eqs. (11) and (12)], and we will keep this assumption unless indicated.

III. WEAK-LOCALIZATION

Although the most dramatic effect of quantum coherence visible in the data of Fig. 1 is the fluctuations of the conductance, we start our discussion of interference effects in ballistic billiards by considering the average conductance, $\bar{G}(B)$, since it is a simpler quantity to analyze theoretically. For a given ballistic microstructure the average can only be defined by summing over some additional variable (such as energy or magnetic field) upon which the conductance is assumed to depend ergodically. The precise definition we choose will be given below. Roughly one may assume that such an average will eliminate all the aperiodic fine structure seen in Fig. 1 leaving any additional smooth dependences on parameters of interest. Following closely our discussion in Refs. 31 and 32, we first show that the leading contribution to the average conductance is classical and then show that there is a quantum correction sensitive to the magnetic field which is analogous to weak-localization in disordered conductors. Such a weak-localization peak has been observed in the ballistic microstructures studied experimentally.[9–11] Very recently a quantitative experimental study of this effect was undertaken;[10] we will compare these experimental results with our calculations at the end of this section.

We start with some numerical results illustrating the effect: Fig. 2 shows $T(k)$ for a half-stadium structure. To reduce nonuniversal effects, we study an asymmetric structure in which a stopper blocks the directly transmitted paths; simpler structures are also discussed below. A natural averaging procedure is to convolve with the derivative of the Fermi function to simulate nonzero temperature. This procedure was applied to the conductance as a function of wave vector for zero and nonzero magnetic field producing the dashed and dotted curves in Fig. 2 (the size of the magnetic field necessary can be seen from the inset). The results show clearly that there is an average magnetoconductance in this structure; the positive sign of the effect is the same as found in disordered conductors.

The average $T(B)$ in the inset of Fig. 2 shows that the ballistic weak-localization effect can be substantial, amounting to as much as 20% of the total average conductance. It also reveals a fascinating new feature unknown from disordered conductors: weak-localization in nonchaotic potentials is qualitatively different from in chaotic potentials. Traces for two structures are shown: a half-stadium structure and a similar structure with straight rather than curved sides. The stadium structure generates

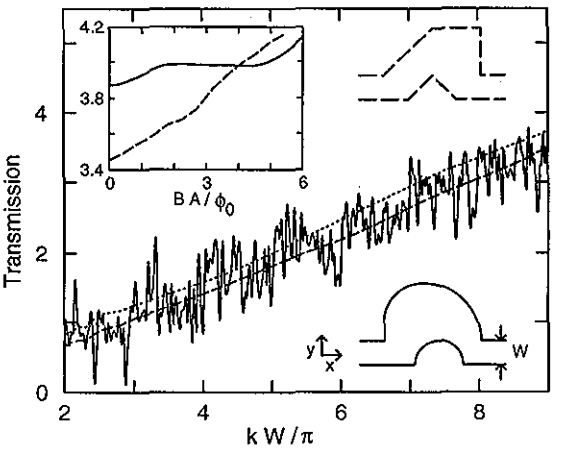

FIG. 2. Transmission coefficient as a function of wave vector for the half-stadium structure shown in the bottom right. The $T=0$ fluctuations (solid) are eliminated by smoothing using a temperature ($T=6$ K for $W=0.5$ μm) which corresponds to 20 correlation lengths. The offset of the resulting $B=2\phi_0/A$ curve (dotted) from that for $B=0$ (dashed) demonstrates the average magnetoconductance effect. Inset: smoothed transmission coefficient as a function of the flux through the cavity ($kW/\pi=9.5$) showing the difference between the chaotic structure in the bottom right (solid) and the regular structure in the top right (dashed). (From Ref. 32.)

chaotic dynamics[38–40] while the polygonal structure does not. (In the polygonal structure the dynamics cannot be ergodic because the angle of a path exiting from the cavity must be related to the angle at entry through reflection from either vertical, horizontal, or diagonal walls.) In the chaotic case the weak-localization effect rises quadratically and then saturates (the subsequent upturn is due to cyclotron effects); whereas the nonchaotic structure shows a *linear* increase with B and no apparent saturation. Hence we immediately obtain a partial answer to one of the key questions posed above: the weak-localization effect apparently allows us to distinguish chaotic from regular dynamics. We now attempt to understand the results, both qualitatively and quantitatively by means of a semiclassical analysis.

A. Semiclassical analysis

Because the classical transmission coefficient is proportional to kW/π, we expect a linear contribution to the average quantum transmission and call the slope $\mathcal{T}$. By averaging $T(k)/(kW/\pi)$ over all k,

$$\langle A\rangle\equiv\lim_{q\to\infty}\left(\frac{1}{q}\right)\int_{q_c}^{q_c+q}dkA(k), \quad \frac{q_cW}{\pi}\gg 1, \qquad (15)$$

one can show[31] that only terms with paired paths, $s=u$, contribute to $\mathcal{T}$. The result of averaging is

$$\mathcal{T}=\frac{1}{2}\int_{-1}^{1}d(\sin\theta)\int_{-1}^{1}d(\sin\theta')\sum_{s(\theta,\theta')}\widetilde{A}_s. \qquad (16)$$

Using the definition of $\tilde{A}_s$, one can change variables from $\sin\theta'$ to the transverse initial position y and arrive at the usual expression for the classical probability of transmission

$$\mathcal{T}=\frac{1}{2}\int_{-1}^{1} d(\sin\theta)\int_0^W \frac{dy}{W} f(y,\theta) \tag{17}$$

where $f(y,\theta)=1$ if the trajectory with initial conditions (y,θ) is transmitted and $f(y,\theta)=0$ otherwise. Thus as expected, the leading order term in the average quantum conductance as the Fermi energy goes to infinity is just the classical conductance.[31]

The weak-localization correction is most easily discussed in terms of the reflection coefficient, $R=N-T$. The quantum corrections to R are

$$\delta R=\frac{1}{2}\frac{\pi}{kW}\left[\sum_n \sum_{s\neq u} F^{s,u}_{n,n}+\sum_{n\neq m}\sum_{s\neq u} F^{s,u}_{n,m}\right] \tag{18}$$

where we have separated out the terms diagonal in mode number, $\delta R_D\equiv\Sigma_{n=1}^{N_M}\delta R_{nn}$, from the off-diagonal terms. From results in disordered conductors,[4] one expects that coherent backscattering will influence $\delta R_D(B)$. In fact, from previous work on both disordered systems[4,41] and quantum-chaotic scattering,[42,43] it is now well-known that a typical diagonal reflection element is twice as large as a typical off-diagonal element when the system is time-reversal invariant. The ratio of mean diagonal to off-diagonal elements is known as the elastic enhancement factor, which is hence equal to 2 in the chaotic case. In the disordered case this effect is referred to as the coherent backscattering peak; unfortunately this term is often used interchangeably with the term weak-localization. A major point of our analysis below is that the weak-localization effect in conductance is not completely explained by the elastic enhancement factor, and there must be additional important off-diagonal correlations present. The same implication was implicit in the theory for disordered conductors but was not to our knowledge explicitly discussed previously. We pattern our discussion of δR_D after previous semiclassical treatments of the elastic enhancement factor.[42–44]

There is a natural procedure for finding the average of δR_D over all k[45] denoted $\langle\delta R_D\rangle$: the sum of N reflection elements each with $|\sin\theta|=|\sin\theta'|$ can be converted to an integral over angle, $(\pi/kW)\Sigma_n\rightarrow\int d(\sin\theta)$. Then, the only k-dependence is in the exponent so that the average eliminates all paths except those for which $\tilde{L}_s=\tilde{L}_u$ exactly.[46] In the absence of symmetry $\tilde{L}_s=\tilde{L}_u$ only if $s=u$, but with time-reversal symmetry ($B=0$) $\tilde{L}_s=\tilde{L}_u$ also if u is s time-reversed. Note that a path and its time-reversed partner will only interfere in δR_D since a path contributing to R_{nm} will enter the cavity at θ_m and leave at θ_n, whereas its time-reversed partner will enter at θ_n and leave at θ_m thus contributing to the *different* coefficient R_{mn} (unless $m=n$ as in δR_D). Thus there is no obvious analog of the effect we are evaluating for off-diagonal reflection.

Introducing a magnetic field in general changes both the classical paths traversed and the action along a given path; however, we will be considering low-field effects in which the change in the geometry of the paths is negligible and only the phase difference which now appears between time-reversed paths is important. For time-reversed pairs this phase difference (which is essentially due to the Aharonov–Bohm effect) arises due to the different sign of the "enclosed flux", $(S_s-S_u)/\hbar=2\Theta_s B/\phi_0$ where $\Theta_s\equiv 2\pi\int_s \mathbf{A}\cdot\mathbf{dl}/B$ is the effective "area" enclosed by the path (times 2π) and $\phi_0=hc/e$. Although we refer to Θ_s as an area, the paths we are considering are not in general closed loops and thus Θ_s is not itself a gauge-invariant quantity. Although we have checked that the statistical properties of Θ_s are gauge-invariant in the chaotic case, it remains to be shown that all aspects of the theory presented below are gauge-invariant. Continuing the argument, we obtain

$$\langle\delta R_D(B)\rangle=\frac{1}{2}\int_{-1}^{1} d(\sin\theta)\sum_{s(\theta,\theta),s(\theta,-\theta)}\tilde{A}_s e^{i2\Theta_s B/\phi_0}, \tag{19}$$

which yields an order unity (k-independent) contribution to $\bar{G}(B)$. Since the average over all k eliminates all but the symmetry-related paths we have shown that the contribution to $\langle\delta R\rangle$ which is diagonal in modes only depends on the interference of paths which are precise time-reversed pairs. This result is *exact* to leading order in k within the semiclassical approximation and does not depend on any specific features of the dynamics beyond the requirement of isolated trajectories. Hence the term *diagonal approximation* in this context refers to the approximation of neglecting possible contributions from off-diagonal reflection coefficients, not to neglecting interference between paths unrelated by time-reversal symmetry. We have shown such contributions vanish in $\langle\delta R_D\rangle$. Equation (19) contains only quantities determined by the classical scattering dynamics, and quantitative evaluation through classical simulations will be briefly discussed below. However, at this point we make a plausible but approximate assumption about the dynamics which allows us to evaluate $\langle\delta R_D\rangle$ explicitly.

If we consider a chaotic system in which the mixing time for particles within the cavity is much shorter than the escape time, the probability of scattering out with any angle θ' is just proportional to the projection of the lead on that direction, $\sin\theta'$. Hence we assume the outgoing distribution is uniform in $\sin\theta'$ for an arbitrary distribution of incoming trajectories. Classical simulations confirm that this is approximately obeyed for the structure in Fig. 2 and improves (as we expect) if the opening to the leads is made smaller. Thus, we replace the sum over backscattered paths in Eq. (19) by an average over all $\sin\theta'$ and find that the resulting expression for $\langle\delta R_D(B=0)\rangle$ is the same as that for $\mathcal{R}$ [which we define in the same way as $\mathcal{T}$ in Eq. (16)]. (Note that $\mathcal{R}$ has the interpretation of the classical reflection probability and can be obtained very accurately from classical simulations.) Alternatively, the assumption of uniformity in $\sin\theta'$ is equivalent to supposing that all R_{nm} are of order $\mathcal{R}/N_M$. Because of the elastic enhancement factor, the diagonal reflection coefficients change by a

factor of 2, and we are again led to the estimation $\langle \delta R_D(B=0) \rangle \approx \mathscr{R}$. To obtain the dependence of δR_D on B, we group the backscattered paths by their effective area and average over the distribution of this area, $N(\Theta)$,

$$\langle \delta R_D(B) \rangle \propto \int_{-\infty}^{\infty} d\Theta N(\Theta) \exp\left[\frac{i2\Theta B}{\phi_0}\right]. \tag{20}$$

Again in obtaining this expression we have assumed that the distribution is uniform in $\sin\theta$ and hence $N(\Theta)$ is independent of θ. Having related $\langle \delta R_D(B) \rangle$ to the classical area distribution we must now evaluate this distribution and the related distributions of lengths.

Before proceeding to this step we note again that this coherent backscattering effect does not contribute at all to the off-diagonal reflection; however, we cannot show that breaking time-reversal symmetry has no effect on the off-diagonal contribution to $\langle R \rangle$. Evaluation of the second term in Eq. (18) is difficult since manipulations of the type used to evaluate $\langle \delta R_D \rangle$ do not yield an expression with k-dependence only in the exponent. Hence the k-average does not eliminate all but paths of the same length and we know of no analytic procedure for evaluating this term explicitly. The naive guess that the absence of exact time-reversed pairs in this term would make it insensitive to the presence of time-reversal symmetry is wrong as demonstrated by our numerical results below.

B. Classical length and area distributions

Both analytic arguments and numerical calculations [2,39,43,47] have found that the area distribution for long orbits takes on a universal form for simple chaotic billiards: $N(\Theta) \propto \exp(-\alpha_{cl}|\Theta|)$, where the only parameter characterizing the classical phase space is the quantity α_{cl} which may be interpreted as the inverse of the typical area enclosed by a scattering trajectory.

The origin of this universal form may be understood qualitatively by the following argument.[39,43,47] First, the number of orbits which remain in the scattering region long enough to cover a distance L decays exponentially with L. Crudely the reason is that for long chaotic orbits the probability of escaping at each encounter with the boundary is a constant $p \ll 1$ given approximately by the ratio of the size of the opening to the perimeter of the billiard and is uncorrelated with previous bounces. Hence after n bounces $P(n) \sim e^{-n\ln p}$, and if d is the mean length traversed between bounces, $P(L) \sim e^{-(L/d)\ln p} = e^{-\gamma_{cl}L}$. A more sophisticated argument relates γ_{cl} to the Lyapunov exponent and dimension of the manifold of infinitely trapped trajectories.[38] Second, the area Θ_s of a given trajectory is essentially given by its winding number around a central point in the billiard times a typical area per circulation A_0 (it is precisely this if the field is replaced by an Aharonov–Bohm flux, as considered by Berry and Robnik[47]). For a chaotic system the area accumulates diffusively, as both senses of circulation occur with roughly equal probability for long orbits. Hence the mean winding number for an orbit of n bounces is zero and its variance $w_n^2 \sim n$.[39,43,47] The distribution of areas for orbits of length L is then Gaussian with the variance $A^2 \approx (L/d)A_0^2$. Finally, in order to obtain the distribution of areas for orbits of all lengths one must integrate this against the exponential distribution of lengths discussed above. The leading behavior of this integral may be obtained by the method of steepest descent[39] since these are rapidly varying functions. One finds then the exponential law for $|\Theta|$ with $\alpha_{cl} \sim \sqrt{\gamma_{cl} d}/A_0$. As an illustration, in Fig. 3 one sees that both the distribution of lengths and effective areas for the stadium billiard are clearly exponential. The square root dependence of α_{cl} on γ_{cl} has been confirmed numerically as well.[39,48]

In contrast to the chaotic case, we do not expect universal forms for the length and area distributions in the regular case. For example in circular billiards typical areas will grow linearly with the length of the trajectory instead of as the square root because a trapped particle never reverses its sense of circulation,[48] whereas in polygonal billiards (as we shall see below) there is a tendency for areas to cancel more completely than in the chaotic case. One generic feature of regular billiards is the existence of families of trajectories which sample phase space very differently over time, and hence one does not expect the length and area distributions to be characterized by a single scale as in the chaotic case. Thus generically one expects power law behavior for these distributions.[48–51] Figure 3 confirms this expectation in the case of the rectangular billiard: we find $P(L) \sim L^{-3}$ for large L and $N(\Theta) \sim \Theta^{-1/2}$ for Θ less than a cutoff value which is smaller than the area of the rectangle (indicating the area cancellation effect just noted).

C. Evaluation of semiclassical $\langle \delta R_D \rangle$

First consider the chaotic case and assume that the exponential form of the area distribution holds for all Θ (an accurate approximation for structures similar to those studied here).[2,52] Performing the integral in Eq. (20) and combining this result with that for the magnitude we obtain a Lorentzian B-dependence:

$$\langle \delta R_D(B) \rangle = \mathscr{R}/[1+(2B/\alpha_{cl}\phi_0)^2]. \tag{21}$$

We emphasize that this is obtained from the semiclassically exact Eq. (19) using two controllable approximations, uniformity and the exponential area distribution. Note that the field scale can be much smaller than one flux quantum through the area of the cavity since the particle may bounce many times before escaping and enclose an area much larger than the area of the cavity.

Now consider the regular case, focusing here on polygonal billiards since these are the type we have studied numerically. We no longer can rely on the uniformity assumption because we expect the distributions to have a significant dependence on the incident angle. We thus are forced to evaluate Eq. (19) by direct simulation, i.e. by injecting classical particles with the appropriate angular distribution and performing the sum over exiting paths with the appropriate phase. The resulting variation of $\langle \cos(2B\Theta/\phi_0) \rangle$ with B is shown in Fig. 3(e). There is a

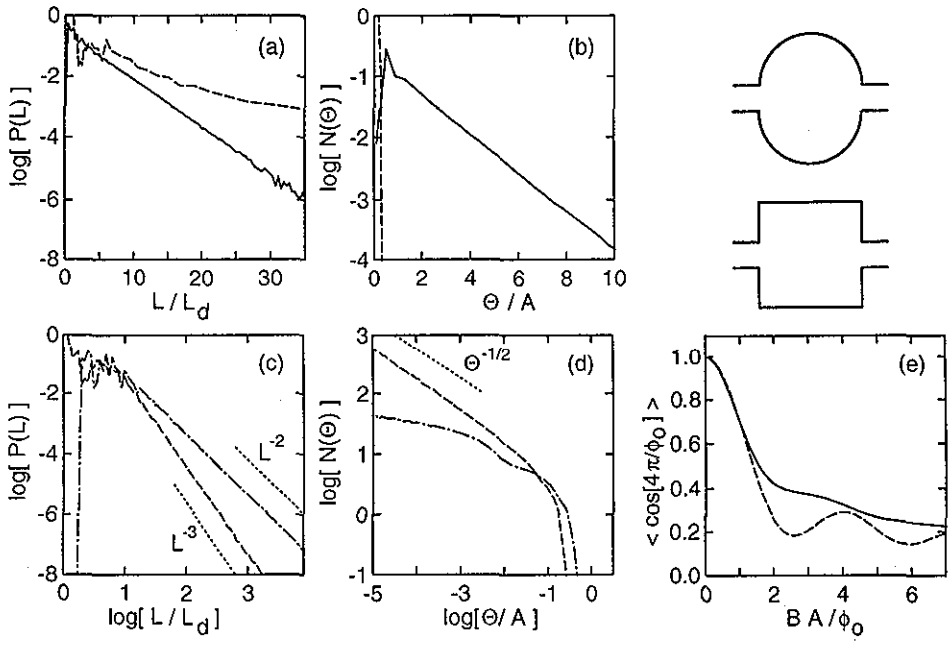

FIG. 3. Classical distributions of length [(a),(c)] and effective area [(b),(d)] for the stadium (solid line) and rectangular (dashed line) billiards shown. (a) and (b) Semilog plot of the distributions: in the stadium both distributions are close to exponential after a short transient region and are very different from the distributions for the rectangle. The exponential distributions are a signature of the single scale characteristic of chaotic systems. (c) and (d) Log–log plot of the distributions in the rectangle show the power law behavior characteristic of nonchaotic systems in which there is a distribution of scales. Different power laws are indicated by dotted lines. In panel (c), the dash-dotted line is the two-particle distribution of length differences [right-hand-side of Eq. (41)]; note that the angular correlations change the exponent. In panel (d), the dash-dotted line is the two-particle distribution of area differences for transmitted particles [right-hand side of Eq. (42)]. Note the cutoff in both the single and two particle distributions at $\Theta \sim A$. (e) The cosine transform of the numerical $N(\Theta)$ (solid) is reasonably well fit by the transform of the function $N(\Theta) \sim \Theta^{-1/2}$ for $\Theta/A < 0.15$ (dashed). The roughly linear dependence for $BA/\phi_0 < 2$ agrees with our quantum result for polygonal billiards (see, e.g., Fig. 2). (A is the area of the cavity; L_d is the direct length between the leads.)

large interval over which the dependence is roughly linear as found in our quantum calculations in Fig. 2 (see also Fig. 5). Some insight into the linear behavior of weak-localization in the polygonal billiards can be obtained from considering the simpler problem of a particle moving ballistically bouncing many times between two planes at $y = \pm L_y/2$. Exactly the kind of phase average needed for Eq. (19) arises in the theory of thin film superconductivity[53] where it was pointed out that all complete traversals between the two planes give zero contribution to the accumulated phase; hence the appearance of parallel walls (combined with ballistic motion) gives rise to a flux cancellation effect, an effect noted earlier in connection with conductance fluctuations.[54] If a path with many bounces begins at $\underline{r}$ and ends at $\underline{r}'$ then only the first and last partial traversal will determine the phase. Assuming these two segments may be treated as uncorrelated one finds $\langle \exp(i\Theta_s B/\phi_0) \rangle = \rho^2(B)$ where $\rho = \langle \exp[i\pi B L_y^2 \times \cot\theta/4\phi_0] \rangle$ where θ is the initial angle and we have assumed the particle starts from $y=0$ for simplicity. Assuming a uniform initial distribution of angles one finds $\rho(B) \sim \exp[-2\pi B L_y^2/4\phi_0]$ which is approximately linear for small B. This argument of course does not take into account the many reflections from the side-walls nor does it apply directly to polygonal billiards without parallel sides. Very recently a periodic-orbit analysis of the rectangular billiard was performed showing that the area enclosed by periodic orbits actually decreases with the length of the orbit,[55] again indicating a very precise flux cancellation in these structures. Hence we believe that these results are very suggestive that flux cancellation is responsible for the linear weak-localization behavior which we find to be generic for polygonal billiards.

D. Off-diagonal correlations

In Fig. 4 we compare the semiclassical predictions for the chaotic case to numerical results. We calculate all the R_{nm} and hence can extract $R_D = \Sigma R_{nn}$. The results for the structure with the stopper are in accord with the semiclassical theory: δR_D is approximately independent of k, its magnitude is within 30% of $\mathscr{R}$, and the elastic enhancement factor is 1.97 ± 0.07 at $B=0$ and 0.99 ± 0.02 at $B/\alpha_{cl}\phi_0 = 2$. We suspect that the deviation of δR_D from the value $\mathscr{R}$ is due to the approximate nature of the uniformity assumption used to go from the semiclassically exact Eq. (19) to Eq. (21); this assumption requires that the escape time be much larger than the mixing time, a condition difficult to achieve numerically in our quantum simulations. Another indication that short paths are important is the net variation as a function of k, which occurs more strongly in the structure with direct transmission paths [Fig. 4(b)] (this structure also shows a smaller weak-localization effect).

In order to test the possibility that the breakdown of uniformity causes the deviation of δR_D from $\mathscr{R}$, we have

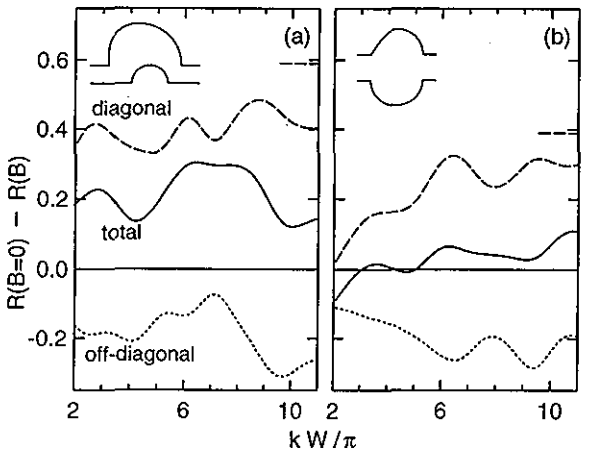

FIG. 4. Change in the total reflection coefficient (solid), as well as the diagonal (dashed) and off-diagonal (dotted) parts, upon changing B from 0 to $2\alpha_c\phi_0$. The curves are smoothed using a window of $1.5kW/\pi$ [30 correlation lengths for panel (a), 15 for (b)]. The dashed ticks on the right mark the classical value of $\mathscr{R}$. Note the roughly k-independent behavior of the curves in (a) and the large contribution of the off-diagonal reflection coefficients to the total weak-localization effect. (From Ref. 32.)

numerically evaluated the classical expression for $\langle \delta R_D \rangle$, Eq. (19), without using the uniformity assumption. Use of an acceptance cone of size ϵ for the exiting angle, $\|\sin\theta'| - |\sin\theta\| < \epsilon$, allows a simple evaluation of Eq. (19). We find that $\lim_{\epsilon\to 0}[\langle \delta R_D(B=0)\rangle - \langle \delta R_D(B=2\alpha_c\phi_0)\rangle] \approx 0.2$. Surprisingly the convergence to the limit is rather slow, requiring $\epsilon \lesssim 0.005$, and the value of this quantity can be substantially larger, of order 0.5, for larger ϵ, presumably because of short trajectories reflecting directly from the stopper. We conclude, then, that uniformity is only approximately obeyed in this structure. Because the value obtained from Eq. (19) is smaller than $\mathscr{R} \approx 0.6$, we expect that the full quantum $\langle \delta R_D \rangle$ will be smaller than $\mathscr{R}$ as observed in Fig. 4.

The most interesting aspect of Fig. 4 is the large change in the off-diagonal terms of *opposite* sign to $\langle \delta R_D \rangle$, a result not anticipated by the semiclassical theory above. *Thus weak-localization is not equivalent to the coherent backscattering (elastic enhancement) effect.* This distinction does not appear to have been appreciated in much of the literature,[31,42–44] including that on disordered systems.[4] The importance of contributions off-diagonal in paths is even more apparent for T since there are *no* time-reversed pairs of paths which contribute to its semiclassical expression. Hence whatever flux-sensitivity is found there cannot be due to interference of classical paths exactly related by time-reversal symmetry.

There is a misleadingly simple argument to understand the decrease in the off-diagonal reflection observed in Fig. 4. The coherent backscattering implies an increase of approximately $\mathscr{R}$ in the diagonal reflection when $B=0$; by unitarity this implies a decrease of $\mathscr{R}$ in the sum of the off-diagonal reflection and the total transmission. Naively this decrease should divide roughly proportional to the probability of reflection vs transmission, i.e. the off-diagonal reflection should decrease by roughly $\mathscr{R}^2$ and the transmission should decrease by $\mathscr{T}\mathscr{R}$. This crude argument is in reasonable agreement with the results of Fig. 4 although it does not indicate how to obtain them semiclassically. However, the same argument gives an absurd result in the disordered case. There $\mathscr{R} \approx 1$, so this line of reasoning would suggest that *all* the enhanced diagonal reflection would be compensated by reduced off-diagonal reflection, leading to zero decrease in transmission and no weak localization effect at all! In fact analytic results show that the decrease in flux needed to compensate the coherent-backscattering comes two-thirds from reflection and one-third from transmission, even though $\mathscr{R}=1$.[41,56] Thus unitarity alone does not explain the off-diagonal correlations in the disordered case.

After discovering the importance of off-diagonal correlations for this problem, we found that this result was implicit in a random-matrix theory approach[57] in which a Hamiltonian from a Gaussian ensemble is coupled to leads to allow scattering. While the elastic enhancement factor has been familiar in various random matrix theories for some time,[58] transport quantities have gained attention only more recently.[59] For good coupling, results in Ref. 57 imply that $\langle \delta R \rangle = 0.25$ in a system for which the elastic enhancement factor yields $\langle \delta R_D \rangle = 0.5 = \mathscr{R}$. Thus an appropriate formulation of random-matrix theory for these systems *does* capture the off-diagonal contributions missed by the diagonal approximation to the semiclassical transmission.

The breakdown of the diagonal approximation (DA) applied to the semiclassical density of states is a longstanding problem in the theory of quantum chaos as discussed by Berry.[23] However for the density of states Berry found that only very long periodic orbits–orbits with periods greater than the Heisenberg time (inverse level spacing)—required abandoning the diagonal approximation. Very recent work[60] has indicated that there are subtle correlations between classical orbits which give rise to contributions to the semiclassical density of states which are off-diagonal in paths and which correct (at least approximately) the failure of the diagonal approximation to describe level correlations at small energies (long times).

However we note that in our cavities the path length is limited by the dwell time, which is much smaller than the inverse level separation, so the off-diagonal interference effects considered in the density of states may not be relevant for the deviations from the DA that we see. Thus our results suggest that a parametrically different scale enters in determining the breakdown of the DA for quantum scattering. In our view it is very much an open question whether the off-diagonal correlations found numerically are describable by semiclassical sums which by definition include only contributions from classical paths. It is worth noting that these correlations in the disordered case can be calculated perturbatively and arise from real-space diagrams which have no representation in terms of purely classical paths.[56]

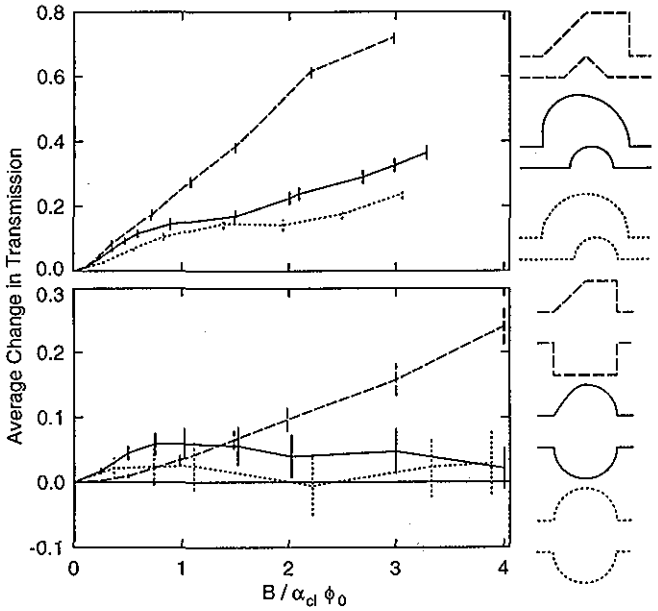

FIG. 5. Weak-localization magnitude as a function of magnetic field for the six structures shown. The magnitude is obtained from $\langle T(k,B)-T(k,B=0)\rangle_k$ with $kW/\pi\in[4,11]$. Note the difference between the chaotic and regular structures, as well as the sensitivity to symmetry in the lower panel. α_{cl} is the inverse of the typical area enclosed by classical paths. (From Ref. 32.)

E. Further numerical results and comparison to experiments

Despite the quantitative inaccuracy of the semiclassical theory of weak-localization presented here, it is successful in certain key respects. It shows that reflection coefficients are sensitive to B through time-reversal symmetry, relates the field scale to the average area enclosed by classical paths, and explains the difference between chaotic and regular structures in terms of the classical distribution of areas.

The semiclassical results suggest analyzing the numerical data by averaging the change in $T(k)$ as shown in Fig. 5. The top panel demonstrates the difference between chaotic and regular structures discussed above: the curves for the half-stadia (chaotic) flatten out while that for the half-asymmetric-square (regular) increases linearly (except for very small B where it is quadratic). As discussed above, we attribute this difference to differing area distributions for chaotic vs integrable structures. Note however that not all of our chaotic structures show a clear saturation; nonetheless all do have rapidly changing magnetoconductance at small field followed by a more gradual rise. We attribute the lack of saturation to the small size of our structures.

The lower panel of Fig. 5 shows that the weak-localization effect is present even for structures without stoppers. The error bars are larger than in the upper panel because of the greater variation with k produced by the direct paths. However, it is interesting, and important for experiments, that the direct paths do not mask the weak-localization effect and the difference between the chaotic and regular cavities is still clear. The lower panel shows an interesting new result: the symmetric stadium shows a much smaller weak-localization effect than the asymmetrized cases. In fact, within the error bars of our numerics we cannot establish that the weak-localization effect is nonzero for this case. However, recent analytic calculations on symmetrized "disordered" systems find that four-fold symmetry reduces but does not eliminate the effect, suggesting that it is indeed nonzero in the chaotic case.[56] The possible role of spatial symmetries in determining $\bar{G}(B)$ was not relevant experimentally for disordered conductors and does not seem to have been explored previously; we now see that it may be experimentally relevant and accessible in the ballistic regime.

Finally, we comment on the relation between our theoretical results and the experiments.[9–11,13–15] As shown above, quantitative extraction of the weak-localization effect from the conductance fluctuations requires an averaging procedure. In experiments this averaging may be achieved either from thermal smearing through the Fermi function or from explicit averaging by varying the potential on a gate which changes the Fermi energy. Thermal averaging was dominant in the earliest experiments,[9] but more recently explicit averaging using a gate has been performed .[10] In either case, the *average* experimental magnetoresistance shows a maximum at $B=0$, in basic agreement with our theory for the existence of weak-localization in ballistic cavities. Of course, because of the conductance fluctuations it is possible to have either a minimum or a maximum at $B=0$ in an *unaveraged* ($T=0$) magnetoresistance trace. In structures with a strong weak-localization signature, we find that about two-thirds of the unaveraged traces show a maximum at $B=0$ while one-third show a minimum, a result roughly confirmed by low-temperature experiments.[61]

Recently Keller *et al.*[10] have investigated weak-localization in detail in a gated structure in which Fermi-energy averages (similar to those employed in our numerics) were possible. The structure employed had a stadium-shaped cavity with off-set leads. In Fig. 6, the experimental results are compared to our numerical results for the asymmetrized-half-stadium with stopper of Fig. 5. Including the factor of 2 for spin, there is remarkable agreement in both lineshape and magnitude when the field is scaled by the appropriate effective area α (extracted from the correlation function of $T(B)$ in the experiment and from classical simulation in the theory). Further work is needed to determine whether this quantitative agreement, which is somewhat surprising in view of the differences between the experimental and theoretical structures, is fortuitous or indicates a large degree of universality in ballistic weak-localization.

Although Marcus *et al.*[9] have studied the difference in fluctuation spectra for circular (integrable) vs stadium cavities (discussed below), no detailed experimental comparison of weak-localization in chaotic and nonchaotic structures has yet been performed. The linear lineshape predicted by our theory for polygonal cavities should be experimentally observable, and we hope such measurements will be undertaken in the near future.

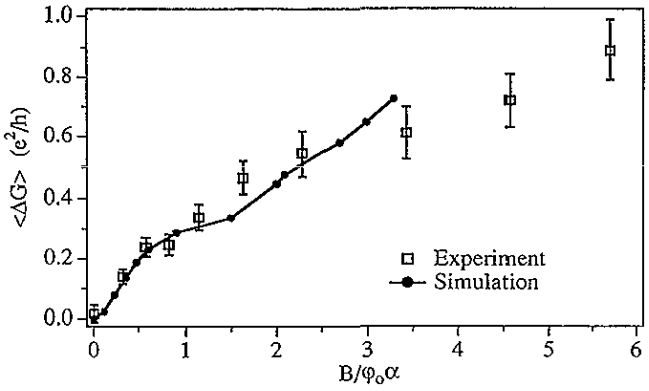

FIG. 6. Comparison of the weak-localization observed experimentally with that obtained numerically for the second structure of Fig. 5. Note the remarkably good agreement between the experimental and numerical values. The experimental points are from Keller *et al.*,[10] and were obtained for a stadium-like cavity with offset leads to eliminate direct paths. The experimental average over k was obtained by varying the gate voltage over a range of $40k_c$. The experimental value of $\phi_0\alpha$ was found by fitting the power spectrum of $T(B)$ to the theoretically predicted form [Eq. (39)]; this value was independent of gate voltage.

IV. CONDUCTANCE FLUCTUATIONS

Fluctuations about the average conductance are characterized by both their magnitude and their power spectrum. We first treat the spectrum of the fluctuations since it is useful in estimating their magnitude; we follow closely our previous calculation of the fluctuations as a function of magnetic field[2] which was based on the semiclassical approach to S-matrix fluctuations as a function of energy introduced by Gutzwiller[62] and extensively developed by Blümel and Smilansky[30] and Gaspard and Rice.[63] We find that the power spectrum can be directly related to properties of the classical phase space and, as was the case for weak-localization, this implies a qualitative difference in the form of the spectrum of chaotic and nonchaotic structures.

A. Power spectrum: Chaotic case

The fluctuations in the transmission intensity are defined by their deviation from the average value studied in the last section; in the absence of any symmetries,

$$\delta T \equiv T - \mathscr{T} kW/\pi. \tag{22}$$

In order to characterize the spectrum of fluctuations, we define the correlation function of the fluctuations in k by averaging over k,[45]

$$C(\Delta k) \equiv \langle \delta T(k+\Delta k)\delta T(k)\rangle_k. \tag{23}$$

The corresponding Fourier power spectrum

$$\hat{C}(x) \equiv \int d(\Delta k) C(\Delta k) e^{ix\Delta k} \tag{24}$$

gives the spectrum of lengths that are important in producing the k fluctuations.

The semiclassical analysis proceeds by an argument similar to that for weak-localization above. First, only part of the correlation function can be treated analytically: in this case the diagonal-approximation consists in the correlation of transmission coefficients between the same modes

$$C_D(\Delta k) \equiv \left\langle \sum_{n,m} \delta T_{nm}(k+\Delta k)\delta T_{nm}(k) \right\rangle_k. \tag{25}$$

The semiclassical expression for the transmission amplitudes, Eq. (6), yields

$$C_D(\Delta k) = \frac{1}{4}\left\langle \left(\frac{\pi}{kW}\right)^2 \sum_{n,m} \sum_{s,u(u\neq s)} \sum_{t,v(v\neq t)} \times F^{s,u}_{n,m}(k+\Delta k) F^{t,v}_{n,m}(k) \right\rangle_k \tag{26}$$

where $F^{s,u}_{n,m}$ is defined in Eq. (14). Because the average is for very large k, we consider the limit when the modes are very dense and replace the sums over modes by integrals over angles. As for weak-localization, the diagonal-approximation yields an expression with k-dependence only in the exponent

$$\langle \exp[ik(\tilde{L}_s - \tilde{L}_u + \tilde{L}_t - \tilde{L}_v)]\rangle_k. \tag{27}$$

The infinite k average implies that the only contribution is for $\tilde{L}_s - \tilde{L}_u + \tilde{L}_t - \tilde{L}_v = 0$ exactly. Because of the definition of C_D in Eq. (25), all four paths satisfy the same boundary conditions on angles, and hence they are all chosen from the same discrete set of paths. In the absence of symmetry, the only contribution is $v=s$ and $t=u$. (The terms with $s=u$ and $t=v$ are excluded because they represent the average values which must be removed from the correlation functions.) Thus we find the exact semiclassical expression

$$C_D(\Delta k) = \frac{1}{4}\int_0^1 d(\sin\theta) \int_0^1 d(\sin\theta') \times \sum_{s(\bar{\theta},\bar{\theta}')} \sum_{u(\bar{\theta},\bar{\theta}')(u\neq s)} \tilde{A}_s \tilde{A}_u e^{i\Delta k(\tilde{L}_s - \tilde{L}_u)} \tag{28}$$

which is independent of k (as discussed further below in connection with the magnitude of the fluctuations). The corresponding expression for the power spectrum is

$$\hat{C}_D(x) = \frac{\pi}{2}\int_0^1 d(\sin\theta) \int_0^1 d(\sin\theta') \times \sum_{s(\bar{\theta},\bar{\theta}')} \sum_{u(\bar{\theta},\bar{\theta}')(u\neq s)} \tilde{A}_s \tilde{A}_u \delta(\tilde{L}_s + x - \tilde{L}_u) \tag{29}$$

where the integral over Δk has been performed.

In the chaotic case, we assume, in a similar spirit to our treatment of weak-localization, that (1) the trajectories are uniformly distributed in the sine of the angle, (2) the angular constraints linking trajectories u and s can be ignored, and (3) the constraint $u\neq s$ can be ignored because of the proliferation of long paths. By averaging over the angles associated with trajectory u,

$$\hat{C}_D(x)=\frac{\pi}{2}\int_0^1 d(\sin\theta)\int_0^1 d(\sin\theta')\sum_{s(\bar{\theta},\bar{\theta}')}\tilde{A}_s \times\int_0^1 d(\sin\theta_1)\int_0^1 d(\sin\theta_2)\sum_{u(\bar{\theta}_1,\bar{\theta}_2)}\tilde{A}_u \times\delta(\tilde{L}_s+x-\tilde{L}_u), \tag{30}$$

and using the identity

$$\delta(\tilde{L}_s+x-\tilde{L}_u)=\int_0^\infty dL\,\delta(\tilde{L}_s+x-L)\delta(L-\tilde{L}_u), \tag{31}$$

one finds that the only remaining constraint on the trajectories is through their lengths. Introducing the classical distribution of lengths

$$P(L)\equiv\int_0^1 d(\sin\theta)\int_0^1 d(\sin\theta')\sum_{u(\bar{\theta},\bar{\theta}')}\tilde{A}_u\delta(L-\tilde{L}_u), \tag{32}$$

we find

$$\hat{C}_D(x)\propto\int_0^\infty dL\,P(L+x)P(L) \tag{33}$$

where x is taken positive. As discussed above, the distribution of lengths is exponential for chaotic billiards for large L, while there may be deviations at small L. Using the exponential form for all lengths, we find that

$$\hat{C}_D(x)\propto e^{-\gamma_{cl}|x|} \tag{34}$$

which is valid for all x since $\hat{C}_D(x)$ must be real and symmetric. This form for the power spectrum implies that the wave-vector correlation function is Lorentzian.[30]

The argument for the magnetic field correlation function[2] is very similar. The correlation function is again defined as an average over k

$$C(\Delta B)\equiv\langle\delta T(k,B+\Delta B)\delta T(k,B)\rangle_k \tag{35}$$

but the difference in action in the phase factors comes from the difference in B. Expanding the change in action to first order in field $[S_s(B+\Delta B)-S_u(B+\Delta B)+S_u(B)-S_s(B)]/\hbar=(\Theta_s-\Theta_u)\Delta B/\phi_0$, we find exactly analogous to Eqs. (28), (29), and (33)

$$C_D(\Delta B)=\frac{1}{4}\int_0^1 d(\sin\theta)\int_0^1 d(\sin\theta')\times\sum_{s(\bar{\theta},\bar{\theta}')}\sum_{u(\bar{\theta},\bar{\theta}')(u\neq s)}\tilde{A}_s\,\tilde{A}_u e^{i\Delta B(\Theta_s-\Theta_u)/\phi_0}, \tag{36}$$

$$\hat{C}_D(\eta)=\frac{\phi_0\pi}{2}\int_0^1 d(\sin\theta)\int_0^1 d(\sin\theta')\times\sum_{s(\bar{\theta},\bar{\theta}')}\sum_{u(\bar{\theta},\bar{\theta}')(u\neq s)}\tilde{A}_s\,\tilde{A}_u\delta(\Theta_s+\eta-\Theta_u), \tag{37}$$

$$\hat{C}_D(\eta)\propto\int_{-\infty}^\infty d\Theta\,N(\Theta+\eta)N(\Theta). \tag{38}$$

Using the known exponential form of the distribution of effective area, $N(\Theta)$, for all values of Θ yields

$$\hat{C}_D(\eta)\propto e^{-\alpha_{cl}|\eta|}(1+\alpha_{cl}|\eta|) \tag{39}$$

for the power spectrum or

$$C_D(\Delta B)=C_D(0)/[1+(\Delta B/\alpha_{cl}\phi_0)^2]^2 \tag{40}$$

for the correlation function. Note for consistency that the field scale of the fluctuations is twice that of weak-localization [Eq. (21)] because the relevant phase involves the difference of two "areas" whereas weak-localization involves the sum.

As in the case of weak-localization discussed above, the terms in the correlation function which are not susceptible to the diagonal-approximation are much more difficult to treat and no analysis of these terms is known at this time. Thus we simply conjecture that the form of the full power spectrum will be the same as that given by the diagonal term. The conjecture is intuitively reasonable since a given property of a chaotic system should be characterized by a single scale which hence should be the same for the full correlation function; we now turn to the numerical results for confirmation of this conjecture.

We have calculated by classical simulations γ_{cl}, α_{cl} and hence can compare the predictions of Eqs. (34) and (39) to exact numerical results for the correlation functions obtained by the recursive Green function method[31] with no free parameters. We consider systems with 4–15 modes at E_F. It is important to note that the semiclassical approximation leading to Eqs. (4) or (6) is not well-justified in the few-mode limit typical of experiments,[9–11] since the difference between the actions of classical trajectories with the same end points is not always much greater than $\hbar$. Thus our numerical results provide a test of the accuracy of the semiclassical approach for determining correlation lengths in this regime.

First we show (Fig. 7) a typical correlation function $C(\Delta B)$ and the prediction of Eq. (40). The agreement is good except in the tail which corresponds to the nonuniversal short trajectory behavior. Because the behavior in the tail affects the half-width, it is necessary to calculate δT from a smoothed $\langle T(B)\rangle$ curve which introduces some arbitrariness in the determination of the correlation field B_c. To eliminate this freedom, we instead extract the correlation area $\alpha_{qm}=\phi_0/B_c$ from fitting the Fourier power spectrum of the data to Eq. (39) (inset to Fig. 7); the value thus extracted is independent of the nonuniversal "low-frequency" behavior.[64] The same approach was used to extract γ_{qm} from $T(k)$ by fitting to the simple exponential power spectrum of Eq. (34). Figure 8 shows the power spectrum for an asymmetrized stadium for two different fillings [see also Fig. 10(a)]. Note that the agreement between the full quantum numerical results and the exponential decay predicted semiclassically is excellent when the number of modes is large—$\log P(x)$ is linear over 4 decades—but is less good in the extreme quantum limit of a single mode—less than 2 decades. The breakdown of

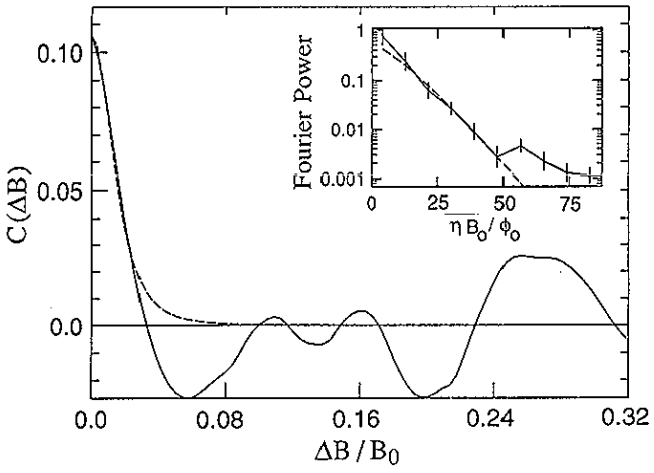

FIG. 7. Magnetic field correlation function for the stadium billiard shown in Fig. 3 (for $W=1000$ Å, half-width $\Delta B_c=4mT$). Dashed line has the form of the semiclassical prediction of Eq. (40). Inset: smoothed power spectrum of $T(B)$. Error bars indicate rms variation of raw data. Dashed line is best fit to Eq. (39) in interval [50,200]. ($B_0=mcv_f/eL_d$ where L_d is the direct length between the leads.) (From Ref. 2.)

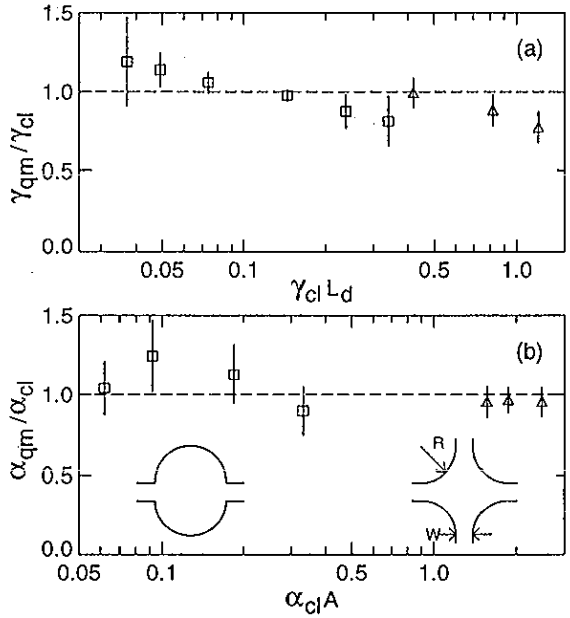

FIG. 9. (a) Ratio of the wave-vector correlation length (obtained by fitting the power spectrum) to the classical escape rate γ_{cl} as a function of γ_{cl} for both types of structures shown. Four-disk structure (triangles) with $R/W=1,2,4$, and stadium (squares) with $R/W=0.5,1,2,4,6,8$. (b) Ratio of magnetic field correlation length (obtained as in inset of Fig. 7) to α_{cl}, the exponent of the distribution of effective areas, as a function of α_{cl}. Four-disk structure (triangles) with $R/W=1,2,4$, and open stadium (squares) with $R/W=1,2,4,6$. The correlation lengths of the quantum fluctuations agree with the semiclassical prediction over two decades. (A is the area of the cavity; L_d is the direct length between two opposite leads.) (From Ref. 2.)

semiclassical theory in the few mode limit is, of course, not surprising and, in fact, has been studied quantitatively in the context of S-matrix fluctuations.[42]

Figure 9 shows that γ_{qm}, α_{qm} are indeed given by the classical quantities γ_{cl}, α_{cl} to high accuracy while they are varied over roughly two orders of magnitude by changing R/W in the two- and four-probe structures shown. *Thus it is possible to predict quantitatively measurable properties of these ballistic quantum conductors from a knowledge of the chaotic classical scattering dynamics.* Indeed, recent experiments[10,13] have investigated the variation of γ_{qm} and α_{qm} with the degree of opening of the cavity. They find the correct trends and quantitatively reasonable values. A detailed comparison of theory and experiment is complicated by the presence of phase-breaking in the experimental structures[13] and by imperfect knowledge of the real potential (see, however, Ref. 48).

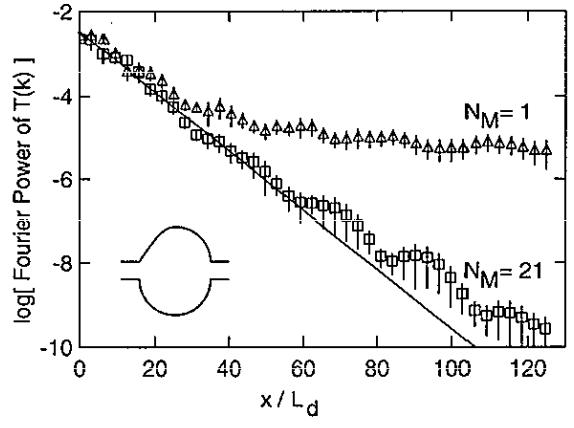

FIG. 8. Power spectrum of $T(k)$ for the chaotic structure shown for two different fillings, $N_M=21$ squares and $N_M=1$ triangles. In the former case, the agreement with the semiclassical theory is excellent; however, in the extreme quantum limit when only one mode is propagating in the leads, there is more high-frequency power and the agreement with the semiclassical theory is much less good.

B. Power spectrum: Non-chaotic case

The semiclassical theory of scattering in nonchaotic structures is presumably related to the treatment of direct trajectories in Sec. II but is less well developed than that of chaotic billiards. Nonetheless, based on the results of the last section, one expects that the spectrum in k or B should be related to the classical distribution of lengths or effective areas for the particles in the cavity. As discussed above, there are at least two basic differences in the nonchaotic case: the trajectories group into families and there is a great deal of angular correlation between incident angle and outgoing angle (the uniformity assumption used successfully in the chaotic case is certainly not valid). Because of these two differences, one expects that the classical distributions will *not* be characterized by a single scale and therefore that these distributions will be power law rather than exponential. As noted above, the results of classical simulations in Fig. 3 confirm this expectation: for the rectangular billiard, $P(L)\propto 1/L^3$ at large L and $N(\Theta)\propto 1/\sqrt{\Theta}$. Though the power law behavior in polygonal billiards is presumably related to the presence of families of periodic orbits and flux-cancellation, a detailed understanding of these power laws is currently not available. It is also pos-

sible that different kinds of nonchaotic structures will show different power laws since there is no *a priori* reason for universality in the nonchaotic case; indeed, results of Lin *et al.* elsewhere in this issue[48] show that the distribution of effective areas in a circular billiard is very different from that found here for the rectangle.

In the absence of a careful semiclassical treatment of conductance in nonchaotic billiards, we develop a conjecture for the spectrum in the nonchaotic case by analogy with the chaotic-billiard results above. From Eq. (29), the power spectrum $\hat{C}_D(x)$ is evidently related to the distribution of two distinct paths with a difference in length of x. In the nonchaotic case, the two distinct paths must come from different families of trajectories and the constraint that the two paths satisfy the same boundary conditions on angles must be retained. Thus we conjecture that

$$\hat{C}_D(x) \propto \int_0^\infty dL \int_0^1 d(\sin\theta)\, P_2(L+x,L,\theta) \qquad (41)$$

where $P_2(L+x,L,\theta)$ is the classical distribution for two distinct trajectories at angle θ, one with length L and the other with length $L+x$. In the chaotic case, this two-particle distribution factorizes into the product of length distributions appearing in Eq. (33) but in the nonchaotic case P_2 does *not* factorize. The classical integral on the right-hand side of Eq. (41) has been computed numerically for the rectangular billiard, and the result in Fig. 3 shows that it decays more slowly than $P(L)$: as $1/x^2$ for large x instead of $1/L^3$.

In the case of the power spectrum of $T(B)$, we assume that a similar expression holds in terms of the classical distribution for two trajectories at angle θ with effective areas Θ and $\Theta+\eta$

$$\hat{C}_D(\eta) \propto \int_{-\infty}^\infty d\Theta \int_0^1 d(\sin\theta)\, N_2(\Theta+\eta,\Theta,\theta). \qquad (42)$$

The result of classical simulation in Fig. 3 shows that this distribution is roughly constant up to a cutoff which is less than the area of the rectangle.

For verification of these conjectured expressions, we turn to the quantum power spectrum for nonchaotic billiards shown in Fig. 10. All three panels show that the nonchaotic structures have more high-frequency power than the chaotic structures: the fluctuations in the nonchaotic case are finer than in the chaotic case.[52] Note that one needs at least 2–3 decades of sensitivity to reliably distinguish the spectra of chaotic and nonchaotic billiards; this indicates the kind of sensitivity necessary for experimental tests. The spectrum of $T(k)$ in the nonchaotic case is indeed a power law: Fig. 10(b) shows that the spectrum is $1/x^2$ at large x within the statistical error. Thus the validity of our conjecture for $\hat{C}_D(x)$ appears to be confirmed. *The difference in the power spectra of chaotic vs nonchaotic billiards (exponential vs power law decay) is explained by the differing classical two-particle distributions of lengths.* On the other hand, because the classical distribution of area is bounded, the conjecture predicts that the spectrum of $T(B)$ should be limited to low frequencies. This is clearly not the case in Fig. 10(c) which looks quite similar to the

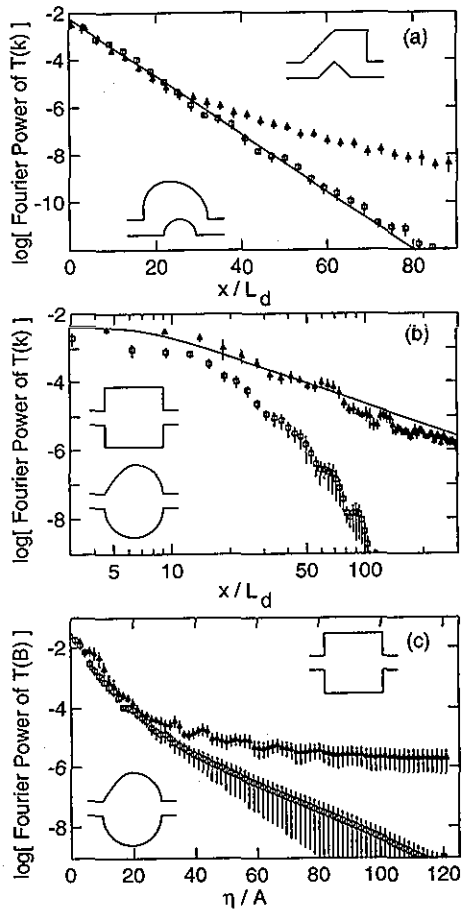

FIG. 10. (a) Power spectra of $T(k)$ for the chaotic (squares) and regular (triangles) structures shown. $N_M=33$. The regular structure has more power at large frequencies because of more trajectories with large lengths. The line is a fit to the spectrum in the chaotic case. The exponential decay predicted semiclassically holds over more than 6 decades. (b) Power spectra of $T(k)$ for a second pair of chaotic (squares) and regular (triangles) structures shown on a log–log plot. $N_M=21$. Again the transport through the regular structure produces more high-frequency power. The spectrum of the regular structure is consistent with the $1/x^2$ spectrum predicted semiclassically and is certainly very different from the spectrum of the chaotic structure. (c) Power spectra of $T(B)$ for the chaotic (squares) and regular (triangles) structures shown. $N_M=6$. The frequency-in-field scale is normalized to the area of the structure, A. The difference between the chaotic and regular structures is apparent in the spectrum of their magneto-fingerprints. This difference has been studied experimentally.[9]

result for the spectrum of $T(k)$ in panel (a). The reason for the failure of our conjecture Eq. (42) is not understood but may well be connected to special properties of the rectangular billiard such as the extreme flux-cancellation effect seen in Fig. 3. Finally, we note that recent experiments *have* observed different power spectra in ballistic microstructures fabricated with circular vs stadium-shaped cavities.[9,15]

C. Scaling of the magnitude

The second property of the conductance fluctuations we study is their magnitude characterized by the variance, $var(T)$. For disordered conductors this quantity was found to have a striking universality, as it was found to be

of order unity independent of the size of the system or the elastic mean free path.[5,6] Our results indicate that a similar scale-independence holds for the fluctuations in the chaotic case. We wish to address the sensitivity of $var(T)$ to the shape of the billiard and the scaling of $var(T)$ with the size of the system at constant shape. In a billiard, the latter is equivalent to the scaling as $\hbar \to 0$ or as $k \to \infty$.

We start by discussing the results of semiclassical theory. The diagonal contribution to the variance can easily be found by setting $\Delta k=0$ in the correlation function Eq. (28):

$$var_D(T)=\frac{1}{4}\int_0^1 d(\sin\theta)\int_0^1 d(\sin\theta') \times \sum_{s(\bar{\theta},\bar{\theta}')} \sum_{u(\bar{\theta},\bar{\theta}')(u\neq s)} \tilde{A}_s \tilde{A}_u. \quad (43)$$

This is a k-independent contribution to $var(T)$ and thus is independent of the size of the system, showing the same kind of universality as in the disordered case. The uniformity assumption can be used to give a simple classical expression for this contribution;[33] the sensitivity of the quantitative value could be investigated by performing the sums over paths in Eq. (43) numerically. Of course, $var_D(T)$ represents only part of the full variance. Evaluation of the off-diagonal part semiclassically meets with the same problems as for the weak-localization and power spectrum: at present the magnitude of quantum transport quantities cannot be quantitatively calculated within the semiclassical diagonal-approximation theory. Thus we turn to numerical results to investigate whether the suggestion of universality implicit in the behavior of $var_D(T)$ is actually realized by the full variance.

In any cavity there are short trajectories which explore only a small part of the available phase space. These trajectories will contribute a nonuniversal amount to the total fluctuations. Thus to make a meaningful comparison of the long-time, possibly universal, contribution to the fluctuations, the contribution of the short paths must be excluded. We do this by fitting the power spectrum to the form derived from the semiclassical theory for long paths (previous two sections) and then use the integral of the fitted power spectrum as our estimate of the variance. We have also considered the variance of the raw data, which is equivalent to the integral of the numerical power spectrum, and find roughly the same behavior but with considerably larger statistical error bars because of the short path contributions.

Figure 11 shows the variance for a stadium structure as a function of the number of modes (which is the integer part of kW/π). Energy averaging is done to obtain each point; the value plotted at point N_M was obtained from data in the range $kW/\pi \in [N_M+0.1, N_M+0.9]$. The variance is independent of the size of the structure (within the statistical error bars) for N_M from 8 to 33. As a check, panel (b) shows that the slope of the power spectrum does not change over this range. *Thus the fluctuation magnitude in a chaotic structure is independent of the size of the structure and is "universal" much as in disordered conductors.*

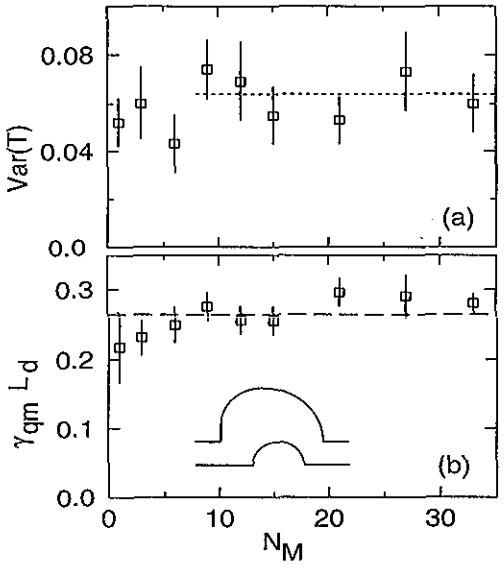

FIG. 11. Variance of the transmission fluctuations [panel (a)] and decay rate of the power spectrum of the quantum conductance fluctuations [panel (b)] as a function of the number of modes in the lead. Both the variance and the decay rate are independent of N_M for large N_M. Thus the fluctuations in a chaotic structure are independent of the scale of the structure, much as in universal conductance fluctuations in the disordered regime. The quantum decay rate agrees with the classical escape rate indicated by the dashed line. $L_d=4W$ is the distance between the leads.

The numerical value of the variance falls in the range 0.065 to 0.14 depending on the structure and seems somewhat smaller than the minimum value 0.133 obtained for disordered conductors (corresponding to the quasi-1-D limit). The small numerical value of the variance in our ballistic structures may be related to the presence of many short paths because of the relative openness of the structures used (pictured in inset).

Figure 12 compares the variance for a chaotic stadium and the rectangular billiard. Again the variance in the chaotic structure is roughly independent of the size. However, for the rectangle the magnitude of the fluctuation rises slowly as the size of the system increases. The data are not sufficient to infer an asymptotic dependence on N_M, and the increase of the fluctuations is not as clear in other regular scattering cavities we have studied. Nonetheless the data suggest strongly that regular cavities do not exhibit universal conductance fluctuations and that this may be a third experimentally accessible transport quantity which differentiates chaotic from nonchaotic quantum scatterers.

For a small number of modes, the magnitude of the fluctuations may in principle show deviations from universality because of the extreme quantum nature of the problem. In fact, our numerical results in Figs. 11 and 12 show only a modest change in $var(T)$ even at $N_M=1$ in the chaotic case, suggesting that $var(T)$ is a very robust quantity indeed. Experiments investigating the scaling of $var(T)$ as the width of the leads is changed have observed a substantial decrease in the magnitude as the number of modes decreases,[11] in apparent disagreement with our results. However, it is likely that a significant amount of

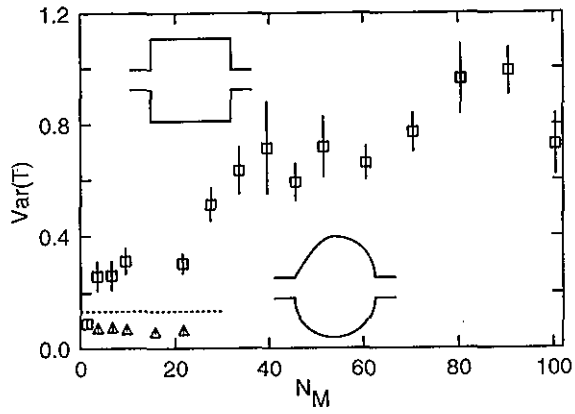

FIG. 12. Variance of the transmission fluctuations as a function of the number of modes for the rectangular (square) and asymmetrized stadium (triangle) billiards. The variance is obtained from fitting the power spectra to the form predicted semiclassically and inferring the variance from the fit. Note the very different behavior in the two cases: the magnitude is nearly constant in the chaotic case while it rises gradually for the rectangle. For comparison purposes the dotted line is the minimum value of the variance for disordered metals (the quasi-one-dimensional case).

thermal smearing is present in these experiments and that the experimental results are therefore not directly comparable to the $T=0$ theory. Comparing the experimental and theoretical results in an equivalent regime remains to be done.

Finally, it is well-known from disordered conductors that $var(T)$ decreases by precisely a factor of 2 when time-reversal symmetry is broken.[5,6] This can be understood from very general properties of the transition between the orthogonal and unitary random-matrix ensembles,[59] and we expect such a result to be valid in the chaotic case as well. Preliminary numerical results indicate that $var(T)$ does decrease with B in chaotic billiards, although further work is needed to determine if the reduction factor is a factor of 2 as expected. We note that it may be possible to test this idea experimentally by, e.g., varying the Fermi energy or shape of the microstructure at zero and nonzero magnetic field.

V. CONCLUSIONS

We have shown that quantum interference effects in the transport coefficients of ballistic microstructures reflect properties of the underlying classical dynamics. If the scattering dynamics is classically chaotic the weak-localization and conductance fluctuations exhibit universal behavior characterized by a single dynamical scale. If the scattering dynamics is nonchaotic then these effects exist but have nonuniversal features and multiple scales. In the chaotic case, semiclassical theory within the diagonal approximation is able to predict the dynamical scales quantitatively from properties of the classical phase-space, but is not able to account for the numerically obtained magnitudes of the effects. The semiclassical theory is suggestive of qualitative differences between chaotic and nonchaotic microstructures, and this is confirmed by numerical results. Specifically, we have studied three effects in which a difference appears: (1) the weak-localization lineshape, (2) the power spectra of the conductance fluctuations in k or B, and (3) the scaling of the magnitude of the fluctuations. However, more careful development of the semiclassical theory for the nonchaotic case is clearly needed. Most importantly, many of the predictions of the semiclassical theory are amenable to experimental test, and we eagerly await the results of the several groups currently engaged in such studies.

In our view the most fundamental remaining problem from the theoretical standpoint is to extend the semiclassical theory to deal with off-diagonal correlations and hence make it quantitative. These correlations were demonstrated in the numerical results above and may be computed analytically in the disordered case[56,65] or through random-matrix theory,[41,57] but are currently out of reach of semiclassical methods. In the disordered case there are indications that these correlations arise from interference between classical and nonclassical paths, suggesting that they are fundamentally beyond the semiclassical approach. However we are not able to say definitively if these correlations imply a fundamental limitation of the semiclassical method or just reflect our present inability to perform the relevant sums.

It is hoped that by clarifying the importance of these off-diagonal correlations our work will stimulate the theoretical community studying quantum chaos to address this unanswered question.

ACKNOWLEDGMENTS

We thank M. W. Keller for help in preparing Fig. 6. We appreciate helpful discussions with M. J. Berry, H. Bruus, E. Doron, M. W. Keller, P. Leboeuf, C. M. Marcus, A. M. Ozorio de Almeida, J.-L. Pichard, U. Smilansky, and B. J. van Wees. The work at Yale was supported in part by NSF Contract No. DMR-9215065 and ARO Grant No. DAAH04-93-G-0009.

[1] For reviews see M. C. Gutzwiller, *Chaos in Classical and Quantum Mechanics* (Springer-Verlag, New York, 1991) and M.-J. Giannoni, A. Voros, and J. Zinn-Justin (editors), *Chaos and Quantum Physics* (North-Holland, New York, 1991).

[2] R. A. Jalabert, H. U. Baranger, and A. D. Stone, Phys. Rev. Lett. **65**, 2442 (1990).

[3] For reviews of mesoscopic physics see C. W. J. Beenakker and H. van Houten in *Solid State Physics*, edited by H. Ehrenreich and D. Turnbull (Academic, New York, 1991), Vol. 44, pp. 1–228; B. L. Altshuler, P. A. Lee, and R. A. Webb (editors), *Mesoscopic Phenomena in Solids* (North-Holland, New York, 1991); and S. Washburn and R. A. Webb, Adv. Phys. **35**, 375 (1986).

[4] For reviews of weak-localization in disordered metals see P. A. Lee and T. V. Ramakrishnan, Rev. Mod. Phys. **57**, 287 (1985) and G. Bergmann, Phys. Rep. **107**, 1 (1984).

[5] P. A. Lee and A. D. Stone, Phys. Rev. Lett. **55**, 1622 (1985); P. A. Lee, A. D. Stone, and H. Fukuyama, Phys. Rev. B **35**, 1039 (1987).

[6] B. L. Altshuler, Pis'ma Zh. Eksp. Teor. Fiz. **41**, 530 (1985) [JETP Lett. **41**, 648 (1985)].

[7] B. L. Altshuler and B. I. Shklovskii, Sov. Phys. JETP **64**, 127 (1986).

[8] N. Argaman, Y. Imry, and U. Smilansky, Phys. Rev. B **47**, 4440 (1993).

[9] C. M. Marcus, A. J. Rimberg, R. M. Westervelt, P. F. Hopkins, and A. C. Gossard, Phys. Rev. Lett. **69**, 506 (1992).

[10] M. W. Keller, O. Millo, A. Mittal, D. E. Prober, and R. N. Sacks, Surf. Sci. in press (1993).

[11] M. J. Berry, J. A. Katine, C. M. Marcus, R. M. Westervelt, and A. C. Gossard, Surf. Sci., in press (1993).
[12] D. Weiss, K. Richter, A. Menschig, R. Bergmann, H. Schweizer, K. von Klitzing, and G. Weimann, Phys. Rev. Lett. **70**, 4118 (1993).
[13] C. M. Marcus, R. M. Westervelt, P. F. Hopkins, and A. C. Gossard, Phys. Rev. B **48**, 2460 (1993).
[14] C. M. Marcus, R. M. Westervelt, P. F. Hopkins, and A. C. Gossard, Surf. Sci., in press (1993).
[15] C. M. Marcus, R. M. Westervelt, P. F. Hopkins, and A. C. Gossard, Chaos **3**, 643 (1993).
[16] N. W. Ashcroft and N. D. Mermin, *Solid State Physics* (Holt, Rhinehart, and Winston, New York, 1976).
[17] R. Landauer, Philos. Mag. **21**, 863 (1970).
[18] M. Büttiker, Phys. Rev. Lett. **57**, 1761 (1986).
[19] D. S. Fisher and P. A. Lee, Phys. Rev. B **23**, 6851 (1981).
[20] A. D. Stone and A. Szafer, IBM J. Res. Dev. **32**, 384 (1988).
[21] H. U. Baranger and A. D. Stone, Phys. Rev. B **40**, 8169 (1989).
[22] M. V. Berry and J. P. Keating, J. Phys. A **23**, 4839 (1990); M. Sieber and F. Steiner, Phys. Rev. Lett. **67**, 1941 (1991); G. Tanner, P. Scherer, E. B. Bogomolny, B. Eckhardt, and D. Wintgen, Phys. Rev. Lett. **67**, 2410 (1991); E. B. Bogomolny, Nonlinearity **5**, 805 (1992); R. Aurich, C. Mattheis, M. Sieber, and F. Steiner, Phys. Rev. Lett. **68**, 1629 (1992); J. P. Keating, Proc. R. Soc. London Ser. A **436**, 99 (1992).
[23] M. V. Berry, Proc. R. Soc. London Ser. A **400**, 229 (1985).
[24] O. Bohigas, M.-J. Giannoni, and C. Schmit, Phys. Rev. Lett. **52**, 1 (1984); O. Bohigas, in Ref. 1, pp. 87–200.
[25] A. Holle, J. Main, G. Wiebusch, H. Rottke, and K. H. Welge, Phys. Rev. Lett. **61**, 161 (1988).
[26] For a review of quantum chaotic scattering see U. Smilansky in Ref. 1, pp. 371–441.
[27] R. A. Jalabert, A. D. Stone, and Y. Alhassid, Phys. Rev. Lett. **68**, 3468 (1992); A. D. Stone, R. A. Jalabert, and Y. Alhassid, in *Transport Phenomena in Mesoscopic Systems*, edited by H. Fukuyama and T. Ando, Springer Series in Solid-State Science (Springer-Verlag, Berlin, 1992), Vol. 109.
[28] A. D. Stone and H. Bruus, Physica B **189**, 43 (1993); A. D. Stone and H. Bruus, Surf. Sci., in press (1993).
[29] T. Ericson, Phys. Rev. Lett. **5**, 430 (1960).
[30] R. Blümel and U. Smilansky, Phys. Rev. Lett. **60**, 477 (1988); Physica D **36**, 111 (1989); Phys. Rev. Lett. **64**, 241 (1990).
[31] H. U. Baranger, D. P. DiVincenzo, R. A. Jalabert, and A. D. Stone, Phys. Rev. B **44**, 10637 (1991).
[32] H. U. Baranger, R. A. Jalabert, and A. D. Stone, Phys. Rev. Lett. **70**, 3876 (1993).
[33] H. U. Baranger, R. A. Jalabert, and A. D. Stone (unpublished).
[34] See, e.g., H. U. Baranger, Phys. Rev. B **42**, 11479 (1990).
[35] J. H. Jensen (preprint, 1993).
[36] W. H. Miller, Adv. Chem. Phys. **25**, 69 (1974).
[37] See, e.g., E. H. Heller in Ref. 1, pp. 547–663.
[38] For reviews of classical chaotic scattering see T. Tél in *Direction in Chaos, Vol. 3*, edited by H. B. Lin (World Scientific, Singapore, 1990), pp. 149–211 and U. Smilansky in Ref. 1, pp. 371–441.
[39] R. Jensen, Chaos **1**, 101 (1991).
[40] M. L. Roukes and O. L. Alerhand, Phys. Rev. Lett. **65**, 1651 (1990).
[41] P. A. Mello and A. D. Stone, Phys. Rev. B **44**, 3559 (1991).
[42] C. H. Lewenkopf and H. A. Weidenmüller, Ann. Phys. **212**, 53 (1991).
[43] E. Doron, U. Smilansky, and A. Frenkel, Physica D **50**, 367 (1991); Phys. Rev. Lett. **65**, 3072 (1990).
[44] R. Blümel and U. Smilansky, Phys. Rev. Lett. **69**, 217 (1992).
[45] It is important to average over an infinite window in k; see Eq. (15).
[46] There are several subtle aspects of this argument which we address briefly. (1) The paths involved in the sum change as a function of k because the boundary conditions on the angles change. This effect is, however, not essential and can be removed by either averaging using a discrete set of $k_n = 2^n k_0$ for which paths always remain in the considered set (though new paths enter, of course), or by inserting a delta-function when introducing the integral over angles and performing the integrals more carefully.[33] (2) Because we are considering the part of R which is diagonal in mode index, the number of paths contributing to the sum increases only linearly with k, and there is no interference between paths which start contributing at some large k_2 and those which were already contributing at $k_1 < k_2$. For instance, the paths contributing to $\Sigma_{n\ \mathrm{even}} R_{nn}(2k)$ are exactly the same as those contributing to $\Sigma_{\mathrm{all}\ n} R_{nn}(k)$ while the paths contributing to $\Sigma_{n\ \mathrm{odd}} R_{nn}(2k)$ are new. Thus δR_D is a simpler quantity than the full two-point correlation function considered, for instance, in the statistics of energy levels in Ref. 23. It is this simplicity which allows an exact evaluation. (3) We assume, of course, that the semiclassical expressions for r_{nm} and R_{nm} converge.[35] Further, we assume that the expression for δR_D converges absolutely in order to exchange the limit $q \to \infty$ and the sum over paths.
[47] M. V. Berry and M. Robnik, J. Phys. A **19**, 649 (1986).
[48] W. A. Lin, J. B. Delos, and R. V. Jensen, Chaos **3**, 655 (1993).
[49] Y.-C. Lai, R. Blümel, E. Ott, and C. Grebogi, Phys. Rev. Lett. **68**, 3491 (1992) and references therein.
[50] W. Bauer and G. F. Bertsch, Phys. Rev. Lett. **65**, 2213 (1990).
[51] O. Legrand and D. Sornette, Europhys. Lett. **11**, 583 (1990); Physica D **44**, 229 (1990).
[52] R. B. S. Oakeshott and A. MacKinnon, Superlat. Microstruc. **11**, 145 (1992).
[53] P.-G. DeGennes, *Superconductivity of Metals and Alloys* (Addison–Wesley, New York, 1966), pp. 255–259.
[54] C. W. J. Beenakker and H. van Houten, Phys. Rev. B **37**, 6544 (1988).
[55] D. Ullmo, K. Richter, and R. A. Jalabert (unpublished).
[56] M. Hastings, A. D. Stone, and H. U. Baranger (unpublished).
[57] S. Iida, H. A. Weidenmüller, and J. A. Zuk, Phys. Rev. Lett. **64**, 583 (1990); Ann. Phys. **200**, 219 (1990).
[58] P. A. Mello, P. Pereyra, and T. H. Seligman, Ann. Phys. **161**, 254 (1985) and references therein.
[59] For a review see A. D. Stone, P. A. Mello, K. Muttalib, and J.-L. Pichard in Ref. 3.
[60] N. Argaman, E. Doron, J. Keating, A. Kitaev, M. Sieber, and U. Smilansky (preprint).
[61] M. J. Berry (private communication, 1993).
[62] M. C. Gutzwiller, Physica D **7**, 341 (1983).
[63] P. Gaspard and S. A. Rice, J. Chem. Phys. **90**, 2225, 2242, 2255 (1989).
[64] Two details of our power spectrum analysis deserve comment. (1) The singularities in the transmission coefficients at the threshold for a mode in the leads[34] produce power at high frequency. Most of the time we work within a given mode (away from threshold) in order to minimize this effect; however, the high-frequency power produced does not hinder our getting the characteristic scale of the fluctuations as in Figs. 7 and 9. (2) We do see low-frequency peaks in the power spectra which, however, are eliminated by averaging in the data shown here in order to reveal the high-frequency behavior more clearly. The connection between the peaks in the power spectrum and periodic orbits in the cavity is not clear (numerically) at this time.
[65] S. Feng, C. L. Kane, P. A. Lee, and A. D. Stone, Phys. Rev. Lett. **61**, 834 (1988).